INVESTIGATING THE IMPACT OF LOCAL WIND CONDITIONS ON TORONTO'S GLASS BALCONY GUARD FAILURES

by

MATTHEW MACKAY HUDSON
B.ENG (MECHANICAL), MCGILL UNIVERSITY, 2013

A MRP presented to Ryerson University

in partial fulfillment of the
requirements for the degree of
Master of Building Science
in the Department of
Architectural Science

Toronto, Ontario, Canada, 2017

Author’s Declaration

I hereby declare that I am the sole author of this MRP. This is a true copy of the MRP, including any required final revisions.

I authorize Ryerson University to lend this MRP to other institutions or individuals for the purpose of scholarly research.

I further authorize Ryerson University to reproduce this MRP by photocopying or by other means, in total or in part, at the request of other institutions or individuals for the purpose of scholarly research.

I understand that my MRP may be made electronically available to the public.

Abstract

Investigating the Impact of Local Wind Conditions on Toronto's Glass Balcony Guard Failures

Matthew Hudson

Master of Building Science (MBSc.), 2017

Ryerson University, Department of Architectural Science

An investigative study was performed on the Shangri-La Hotel in Toronto in order to determine the impact of local wind conditions on the glass balcony guard failures seen in Toronto in the last five years. An accurate CFD simulation model was developed for external flow applications through a wind tunnel validation study. The simulation was used to analyze average wind conditions and extreme (gust) wind conditions at the balcony guard failure locations, as well as identify potential areas of concern on the Shangri-La Hotel. A strong correlation between failure location and common wind conditions was established, however it was concluded that wind loading was likely not the primary cause of failure.

Acknowledgements

Thank you to the faculty and staff in the graduate program of Building Science at Ryerson University. In particular, the technicians and staff in Ryerson's Fabrication Lab who helped to create the wind tunnel model.

A special thank you to Dr. Ramani Ramakrishnan for supervising the project, providing thoughtful insight, and valuable guidance throughout the MRP process.

Finally, thank you to my family and friends for their continued support throughout my educational career and life endeavours.

Contents

Author's Declaration........ii
Abstract........iii
Acknowledgements........iv
List of Tables........vii
List of Figures........viii
1. Introduction........1
2. Literature Review........2
  2.1 Wind Engineering – Induced Pressures and Failure........2
  2.2 Glass Failure Mechanisms........4
  2.3 Wind Tunnel Testing........7
  2.4 Computational Fluid Dynamics (CFD)........9
  2.5 Summary........12
3. Background........13
  3.1 Balcony Guard Failures in Toronto........13
  3.2 Balcony Guard Failures at The Shangri-La Hotel........15
4. Methodology........17
5. Validation Study........18
  5.1 Wind Tunnel Study........18
    5.1.1 Scaling........18
    5.1.2 Equipment and Data Acquisition........18
    5.1.3 Wind Tunnel Calibration........20
    5.1.4 Wind Tunnel Model........23
    5.1.5 Results........26
  5.2 CFD Study........30
    5.2.1 Set-Up: Autodesk CFD........30
    5.2.2 Sensitivity Analysis........33
    5.2.3 Summary........45
6. CFD Analysis of the Shangri-La Hotel........48
  6.1 Historical Wind Data Analysis........48
  6.2 Set-Up: Autodesk CFD........51
  6.3 Results and Discussion........57
7. Conclusion........66
Appendices........68

Appendix A 68
Appendix B 69
References 70

List of Tables

Table 1: Selection of glass in a guard (OBC Supplementary Standard SB-13, 2012)................14
Table 2: Failure location information 16
Table 3: Data acquisition settings...20
Table 4: Calibration constants for tested input frequencies 22
Table 5: Model dimensions and blockage ratio...24
Table 6: Trial 1 finite element summary...34
Table 7: Trial 2 finite element summary...36
Table 8: Trial 3 finite element summary...39
Table 9: Trial 4 finite element summary...41
Table 10: Final simulation finite element summary..43
Table 11: Sample difference between experimental and simulated results over all trials...........45
Table 12: Historical wind analysis summary...50
Table 13: CFD simulation scenarios...50
Table 14: Values of gradient height and power law exponents for wind profiles [33] 54
Table 15: Wind speed at failure location height...56
Table 16: Finite element summary 57
Table 17: 70° CFD results 59
Table 18: 220° CFD results..61
Table 19: 250° CFD results..64
Table 20: Wind tunnel experimental data 68

List of Figures

Figure 1: The Shangri-La Hotel, rendering (A), location (B)......15
Figure 2: Failure location photographs......16
Figure 3: Failure locations, South elevation (A), East elevation (B)......16
Figure 4: Wind tunnel, open (A), closed (B)......19
Figure 5: Location of calibration pressure measurements......21
Figure 6: Wind tunnel model with pneumatic connections......23
Figure 7: Sketchup representation, 0° orientation (A), 10° orientation (B)......23
Figure 8: Mounted wind tunnel model (C)......24
Figure 9: Model balcony geometry......25
Figure 10: Pressure tap locations......25
Figure 11: Standard deviation, all measurement locations, 0° orientation at 20 Hz......26
Figure 12: Measurement location 4 experimental data......27
Figure 13: Measurement location 8 experimental data......27
Figure 14: Wind tunnel experimental results, 0° orientation at 20 Hz......28
Figure 15: Wind tunnel experimental results, 10° orientation at 20 Hz......29
Figure 16: Wind tunnel experimental results, 20° orientation at 20 Hz......29
Figure 17: Wall layer mesh enhancement......32
Figure 18: Autodesk CFD convergence plot example......33
Figure 19: Trial 1 meshing and results......34
Figure 20: Trial 1 - Software default settings......35
Figure 21: Trial 2, mesh refinement of balconies......37
Figure 22: Trial 2 - Manual mesh refinement......38
Figure 23: Trial 3 - Mesh adaptation......40
Figure 24: Mesh adaptation, final cycle......41
Figure 25: Trial 4 - Modified turbulence model......42
Figure 26: Trial 5 - Final simulation......44
Figure 27: Wind rose (YTZ airport), July 2012 to July 2014 (radial units: hours)......48
Figure 28: Gust condition, January 24th to 31st, 2014......49
Figure 29: Simplification of 3D massing geometry, original (A), simplification (B)......51
Figure 30: Simplification of the of Shangri-La Hotel 3D massing geometry, original (A), simplification (B)......52
Figure 31: Recommended dimensions of external volume......52

Figure 32: Velocity profiles, CFD inlet boundary condition 55
Figure 33: CFD model with boundary conditions 55
Figure 34: Balcony mesh refinement, nodes (A), pressure results with mesh (B) 58
Figure 35: 70°, gust condition 59
Figure 36: East facade, floor 51 failure location 60
Figure 37: 220°, gust condition 61
Figure 38: Plan view, floor 51 (A), floor 23 (B) 62
Figure 39: South facade, gust condition 63
Figure 40: 250°, gust condition 64
Figure 41: Southwest, gust condition 65
Figure 42: Wind tunnel specifications 69

1. Introduction

In the building industry, the use of the word “sustainability” can imply many things, however it is often defined as “the capacity to endure.” The premature failure of building components, leading to ongoing maintenance, replacement, and restoration, is a very unsustainable issue in the buildings of today, and must be considered and evaluated. The cause of failure must be investigated through research and forensic analyses in order to understand the failure mechanism and improve design practices, thus reducing the probability of future occurrences.

The purpose of this paper is to investigate the failure of glass balcony guards seen in Toronto’s high rises in the last five years. Specifically, this paper will aim to answer the following research question: What is the impact of local wind conditions on glass balcony guard failures? There are many potential causes of this recent phenomenon seen in Toronto’s high rises, however the primary focus of this paper is the role of local wind conditions and the potential of the intensification of these conditions due to the surrounding urban environment. Urban environments, with many densely packed high rises, often produce regions of high wind speed (“wind tunnels”) between buildings. It is hypothesised that there is a correlation between the areas of intensified wind loading and the location of balcony guard failures, which would support the theory that wind loading does in fact play a role in these balcony guard failures.

In addition, the following specific objectives will be addressed:

- Establish an accurate and reliable CFD model for an external flow application through a wind tunnel validation study
- Investigate the proposed research question through a case study of the Shangri-La Hotel in downtown Toronto
- Identify potential regions of concern on the Shangri-La Hotel’s façade that should be considered for increased frequency of inspection and maintenance
- Develop a simple methodology which can be used to evaluate the local wind effect on an urban region or neighbourhood, and identify potential areas of concern

In order to begin to address and investigate the topics discussed above, a literature review must be performed which explores material failure due to wind loading, and specifically of the fatigue failure mechanics of glass. The various methods used to evaluate and analyze these material failures, including wind tunnel testing and computational fluid dynamics (CFD) techniques must also be explored and understood.

2. Literature Review

2.1 Wind Engineering – Induced Pressures and Failure

Wind engineering has historically been a topic of interest and necessity for engineers, architects and all other professions involved in the built world. The study of wind and its interaction with the surrounding environment and landscape provides useful and critical information for many applications. In civil engineering, wind conditions are primarily assessed for structural considerations to ensure the building or structure can withstand loading produced by extreme winds. Wind studies are also performed to assess acoustic conditions such as occupant discomfort due to noise generation by wind, and pedestrian comfort at street level due to increased wind speeds in urban areas. In the renewable energy sector, feasibility studies are performed to assess locations for potential wind turbine installation. Wind studies are not only performed in the built world, but in the natural world as well. For example, Dupont [1] developed a model to predict the probability of tree damage in a forest due to strong intermittent wind gusts. The model was based on a coupling between a statistical wind speed model at tree canopy level generated with meteorological data from a nearby weather station, and an existing tree swaying model.

In many cases, the objective of a wind based study is to accurately predict the wind induced pressures on a surface or object. The impact of the pressures on the potential failure of the subject of interest can then be analyzed and explored. Wind conditions are a source of fatigue stresses on materials, which causes the weakening of the material due to repeatedly applied loads (or cyclic loading). Extreme wind conditions that produce intense, short term pressures are also considered. Generally, two types of wind pressure studies are performed: static and dynamic studies. Static wind pressures are evaluated to determine the impact of steady state conditions. Static studies can be useful for evaluating average or common wind conditions. While dynamic wind studies are used to analyze the effect of changing, variable wind conditions.

A key part of sustainable building design is the use of durable materials, or long life building technologies, to reduce or eliminate the need for routine maintenance and replacement of building components. Effects of cyclic loading must be considered for all building components and materials exposed to the wind. Sealants used between building materials to block the passage of water and air are often subjects of premature failure due to cyclic loading. Sealant is often not only exposed to the elements, but also to the stresses caused by the relative movement of the materials on which it is applied. Wind forces have an effect on both of these factors. The resistance to fatigue stresses of a double sealant technology was explored by Ihara, Gustavsen & Jelle [2]. Sealant was applied to aluminum plates and was put through extension and compression cycles to simulate fatigue stressing. It was found that the fatigue resistance of the sealant joint is strongly correlated to the sealant depth and the relative movement of each type of sealant. Optimal section dimensions of sealant exist for any unique case that provides the highest fatigue resistance.

Studying the impact of wind pressures on failure is also important in locations that frequently experience extreme storms, such as hurricanes or cyclones, that generate very high wind speeds. A topic of frequent discussion is the impact of high wind loads on roof assemblies and their components. Studies are often performed as large or full scale experiments. Mooneghi, Irwin & Chowdhury [3] performed an investigative study on the wind loading of flat roof concrete pavers, to determine the uplift forces under extreme wind conditions. Wind conditions were simulated in the “Wall of Wind” open jet facility at Florida International University at critical direction that generates vortices at the corners of the roof. Corner vortices result in suction forces along the flat roof surface. It was found that increasing the pavers edge-gap to spacer height ratio improves the behaviour, and the ratio of spacer height to parapet height must also be considered.

A topic of recent discussion has been the impact of wind loading on photovoltaic (PV) systems. The efficiency of these PV systems decreases drastically when the crystalline structure of the modules is damaged by climatic conditions such as the wind [4]. PV systems often require careful structural considerations, especially when mounted on building rooftops where module racking systems and anchoring into the roof structure is required. Large ground mounted arrays also require careful consideration of the aerodynamic loads and wind flow generated around the system. Utility scale ground mounted arrays (or “solar farms”) are typically very large in size, and therefore have a significant impact on the wind flow in the surrounding areas. For instance, PV arrays installed in close proximity to highways should not have the potential to cause turbulent wind conditions for passing by vehicles. A computational fluid dynamics (CFD) approach was taken by Jubayer & Hangan [5] to investigate the wind load and the underlying aerodynamic mechanism responsible for wind loads on a ground mounted PV panel array. The study investigated the effect of straight and oblique wind directions on a typical solar array. In addition, the effect of module row spacing, module inclination and module dimensions on the wind loads should be explored.

Objects moving through air, such as vehicles, must also be subject to these types of studies. Vehicles create, and are subject to, the same forces and pressures as those created by the wind. The term for the piece of glass in the front of a vehicle is “windshield.” In reality, it is not shielding the vehicle occupants from the wind, but from the forces created by the vehicle moving through the surrounding air, in addition to the wind. As the velocity of the vehicle increases, the induced pressures become more severe and the studies become increasingly important. Consideration of these factors in aircraft material and component design is critical. Due to the nature of a moving vehicle, these studies are often dynamic studies which evaluate the effect of acceleration and change in direction of the vehicle. However, in the case of aircraft, which experience extended durations of unchanging conditions, static studies must also be performed on the fatigue resistance of components due to cyclic loading. Removable joints such as rivets, pins, bolts and other connections are the most important elements in aerospace structures. The forces and pressures applied to these components due to cyclical loading is frequently explored due to safety considerations. Esmaeili, Chakherlou & Zehsaz [6] studied the effect of torque tightening on the fatigue strength of aircraft grade double lap bolted joints. It was found that higher torque levels or clamping force of the joint leads to an improvement of the fatigue strength of the component due to induced compressive stresses around the hole.

Regardless of the application, the objective of wind based studies and fatigue failure studies are the same in all cases: accurately represent the local conditions and resulting forces to analyze the parameter of interest. In order to do this, various tools such as wind tunnels and computational fluid dynamic (CFD) software can be used, and an in depth knowledge of fluid dynamics is required.

2.2 Glass Failure Mechanisms

Glass is one of the most widely used materials in the world and is used in many different applications including its use in the building industry as glazing, cladding, decorative features, or as a structural material. Glass is characterized as being a very brittle material and its failure often poses a risk to public safety, which is why it’s failure is a topic of wide discussion. Glass failure is also unique in the fact that it can be very unpredictable and inconsistent, due to various manufacturing techniques, installation procedures and inevitable presence of cracks and defects within the specimen. Therefore, it is very difficult to define a guaranteed strength for different types of glass. Research was performed in the fields of material failure and fracture mechanics, specifically in the fracture mechanics of tempered glass.

Methods and processes, such as lamination and thermal tempering, exist to increase the strength of glass and alter its mode of failure to limit public safety risks. Thermally tempering glass is a method to improve the impact and fatigue resistance of the specimen by introducing residual compressive stresses into the surface layer, and tensile stresses in the center regions [7]. This is done by heating the specimen to it's state transition temperature, and then rapidly cooling it with forced air drafts. In theory, the residual compressive surface stresses induced in the tempering process will act as a crack closing mechanism, strengthening the surface of the glass. When thermally tempered glass fails, it shatters into very small pieces as opposed to shards, improving safety concerns.

As previously mentioned, it is difficult to define a failure strength for tempered glass, but values are often calculated experimentally in studies such as on performed by Veer, Louter, & Bos [8], in which failure stresses of fully tempered glass was reported in the range of 98.0 MPa (standing) to 157.4 MPa (lying). A study performed at Rutgers University [9] considered the effect of static loading versus cyclic loading over an extended period of time (fatigue loading) up to 10^7 seconds (approximately 116 days). For a static loading condition over this duration, the failure strength of glass decreased from approximately 90 MPa to 45 MPa. While cyclic loading, at a frequency of 10,000 Hz, produced an initial failure strength of approximately 76 MPa. The study [9] also considered the fatigue behaviour of annealed glass versus tempered glass. It was found that tempered glass had an initial failure strength of approximately 240 MPa, and a failure strength of 170 MPa after a fatigue loading duration of 10^6 seconds.

However, in both of the discussed studies samples without imperfections were used, and as such the reported strength values do not take into consideration the effects of cracks and defects in the material. Due to this, practical strength is almost always much less than theoretical strength for glass. In contrast to annealed glass, an embedded crack in the interior layers of tempered glass may spontaneously propagate due to the residual tensile stresses induced during the tempering process [7]. Edge quality also becomes a critical factor for tempered glass, as any edge damage will likely result in an eventual failure of the specimen.

Fracture mechanics is the study of the propagation of cracks in materials, and is a widely discussed topic for glass. Small cracks are often present in new specimens of tempered glass, incurred during manufacture, transportation or installation, or can develop over time due to induced stressing from impurities, such as nickel sulphide inclusions or stones. One of the most widely discussed crack inducing impurities in tempered glass are unintentional nickel sulphide (NiS) inclusions. NiS inclusions can cause embedded cracks to occur in tempered glass. Nickel sulphide is a crystalline polymorphous compound and occurs in two polymorphic modifications: low temperature modification (β-NiS) and a high temperature one (α-NiS) [10]. During the rapid cooling stage of the tempering process, the embedded NiS is unable to transition back to its low temperature β-NiS modification. Since the high temperature α-NiS modification is an unstable state at room temperature, it will eventually transition back to its low temperature β-NiS modification. However, this transition can occur over a period ranging from several hours to several years, and is associated with a volume growth rate of 2% to 4%. The growth of the NiS inclusion can produce surrounding micro cracks, which can cause the spontaneous breakage of tempered glass. The risk of this occurring is increased if the inclusion is located in the tensile stressed center region of the glass.

The effect of impurities and the degree of temper on the failure of tempered glass under stresses lower than the admissible value was studied by Chang & Chou [11]. Impact, bending and static pressure experiments were performed on tempered glass specimens of 210 mm by 290 mm and thicknesses of 4.5 mm and 8.0 mm. With a degree of temper of 0.9 N/cm and 2.0 N/cm, breaking strength under the static pressure test was 0.89 kg/cm (87.3 kPa) and 4.5 kg/cm (441.3 kPa), respectively. Tempered glass samples with various impurities (gas bubble, alkali bubble and stones) were then tested in a thermal shock experiment. It was found that out of 110 tested samples with stone impurities, 63.6% (70 samples) fractured. The impact of the location of the stone impurity within the glass on the sample failure was also explored. With the stone impurity located within 2.1 mm from the surface of the glass (compressive layer), no failures occurred in a 200 sample experiment. However, when the stone impurity was located in the tensile layer (2.15 mm to 5 mm depth in glass), 70 out of 110 samples (63.6%) failed. The conclusion was made that when certain impurities exist in the tensile layer, samples will fracture under external forces lower than the admissible value. The same conclusion was made by Le, Song, & Peng [7]. Below certain ratios of crack size to thickness of glass, thermally tempering glass will hinder crack propagation. However, as crack sizes increase, and depending on location and degree of tempering, the central tension inside tempered glass will cause cracks to become unstable and propagate spontaneously.

The degree of temper also has an impact on the failure of tempered glass samples with embedded impurities. In general, increasing the degree of temper results in an increase of the residual tensile stresses in the interior region, and an overall increase in strength. However, Chang & Chou [11] found that when impurities are present in the interior region, the increase in tensile stresses also correlates to an increase in the stress concentration around the impurity location, which can result in crack propagation and spontaneous failure.

The failure of tempered glass is a complex matter that has become a subject of interest to the general public due to the rare phenomenon of “spontaneous” failure.

2.3 Wind Tunnel Testing

Historically, especially before modern advancements in CFD software, and to this day wind tunnel testing has been a very important tool in all industries involving aerodynamics, such as aerospace, automotive and civil engineering. Wind tunnels provide an experimental method to study and analyze how air moves around solid objects by using a powerful fan system. In civil engineering, wind tunnel testing is important for structures with large or complex geometries, such as high rise buildings and long-span bridges. Many people believe that the increase in the use of wind tunnel based studies was originally initiated by the wind induced 1940 collapse of the Tacoma Narrows Bridge. Large structures often produce load conditions which are hard to estimate, and therefore standardized building codes are not applicable. For example, an extensive wind tunnel study was recently performed by RWDI Consulting Engineers and Scientists on a proposed 80-storey building in downtown Toronto [12]. This study was done to predict the wind pressure distributions along the height of the building, to aid in the design of features to diffuse the wind load, and most importantly to design the tuned mass damper that will be used in the building. Tuned mass dampers are used in very tall buildings as a counter weight to reduce the building’s natural wind induced movement.

There are many different types, sizes classifications of wind tunnels, based on the application and purpose. The two main types are: closed return and open return tunnels, each designed with a specific speed range. In closed return wind tunnels, air is pulled through the test section by a fan system and continuously circulated through the ductwork. Whereas, in an open return design, air is collected from the space in which the wind tunnel is located, accelerated through the test section by fan system and deposited back into the space [13].

Wind tunnel testing of the urban environment and buildings can be important in predicting extreme wind loading, especially in hurricane regions. In order to produce a flow that accurately represents a local wind condition, several factors must be taken into account. Wind tunnel testing of structures is unique because of the critical flow region between the ground surface and the air above, called the planetary boundary layer. Here, the earth’s terrain roughness slows the wind near the ground which results in an increase in wind velocity with height (i.e. there is wind shear) [14]. The approaching flow can also be affected by surrounding buildings and other structures. This region must be accurately represented in the wind tunnel in order to produce reliable and accurate results. Simulation of the approaching flow is typically achieved in experimentation with a combination of flow devices, such as spires at the test section inlet, followed by a length of roughness elements on the test section floor, representing terrain roughness [15]. The specifications of setups such as this are explained in detail in standards such as “Wind Tunnel Testing for Buildings and other Structures” by the American Society of Civil Engineers (ASCE) [15].

Since the objective of most wind tunnel studies is to replicate realistic scenarios and conditions, the physical constraints and boundaries of the wind tunnel must be taken into consideration. In a closed section wind tunnel, the walls represent a physical boundary, which has a significant affect on the behaviour of the flow if not accounted for. If the test model is close enough in proximity to the wind tunnel walls, the flow will be accelerated through this region, producing an unrealistic flow condition, known as the “blockage effect” [16]. Blockage effect can lead to errors in the measurement of forces and pressures on the test model. Errors can be minimized, or even eliminated, by reducing the test model size as much as possible.

The “blockage ratio” is the ratio of the projected cross sectional area of the model to the cross sectional area of the test section, expressed as a percent. In order to minimize the blockage effect, this number must be as low as possible. In general, it is recommended to maintain the blockage ratio below 10% [15]. On the other hand, the ASCE standard recommends a blockage ratio of 5% or lower. When blockage ratios exceed this number, corrections must be made in the data analysis to account for this effect.

There are many different types of wind tunnel studies related to buildings, each with different measurement techniques and test methods. Studies include: determining the wind load on the building’s structural system, aeroelastic testing, pedestrian level wind speeds, and testing to determine the cladding loads. The test method of concern in this paper, determining cladding loads, consists of a rigid model that is instrumented with many pressure taps (up to several hundred) connected via tubing to electronic pressure transducers. These taps measure external pressures exerted at these points by converting the pressures to electrical signals which is then measured by a data acquisition system [17]. An example of this type of wind tunnel study was performed by Chand, Bhargava, & Krishak [18]. Wind induced pressures were measured on a 1:30 scale model of a five storey building with and without balconies in order to analyze the effect on ventilating inducing wind forces. An atmospheric boundary layer was generated with a combination of three devices: vortex generators, a grid of horizontal rods and a set of roughness elements on the floor of the test section. 45 pressure taps were distributed across the surface of the model and measurements were performed with a scanning valve and a digital micro-manometer.

Today, wind tunnel testing is required for certain types of studies and provides an accurate and tangible experimental method for analyzing air flow. However, for many types of studies, wind tunnel testing represents an unnecessary allocation of time and money, where equally accurate solutions can be reached with computational fluid dynamic (CFD) software simulations.

2.4 Computational Fluid Dynamics (CFD)

Computational fluid dynamics (CFD) software uses numerical analysis and algorithms to solve, represent and analyze various fluid (gas or liquid) flow scenarios. CFD software has become increasingly popular in the field of fluid dynamics, as the accuracy of the solutions improves and improvements in computing power, and therefore the computational requirements of running the software, continue to be made. A historical limitation with the use of CFD software is its direct relationship to the computing power of the machine it is being run on. CFD simulation was limited to large high speed super computers owned by research groups or large companies. With modern advancements in computing, and in the solvers of the software, many types of CFD simulations can be solved on personal computers and laptops. However, the case can still be made that the accuracy of the solution reached by the CFD software is only as powerful as the machine it is run on. It also must be recognized that many different versions of CFD software's exist today, some of which are less accurate or robust than others.

In many cases, the use of CFD software over wind tunnel testing is preferable due to the savings seen in time and money. Also, unlike wind tunnel testing, CFD does not suffer from potentially incompatible similarity requirements because simulations can be conducted at full-scale [19]. However, the reliability of CFD software is still at a stage where wind tunnel studies are often required in order to perform an initial experimental validation study. CFD software can be used to simulate the flow of many types of gases and liquids in various flow scenarios, such as internal or external, turbulent or laminar, and supersonic or subsonic flow.

All CFD software follows a similar solution methodology to simulate the interaction of the fluid of interest with volumes or surfaces. After the user has completed the solution set-up, a preprocessing stage is initiated, where the geometry is defined, the volume occupied by the fluid is divided into discrete cells (the mesh) and the boundary and initial conditions are defined. The computing machine then performs the calculations in an iterative process. The fundamental basis of these three dimensional calculations, and modern CFD software, are the Navier-Stokes equations. The Navier-Stokes equations apply to a viscous, heat conducting fluid and consists of the continuity equation (1), the momentum equation (2), and the energy equation (3).

$$\frac{\partial \rho}{\partial t} + \frac{\partial}{\partial x_j}\left[\rho u_j\right] = 0 \tag{1}$$

$$\frac{\partial}{\partial t}\left(\rho u_i\right) + \frac{\partial}{\partial x_j}\left[\rho u_i u_j + p\delta_{ij} - \tau_{ji}\right] = 0, \quad i = 1,2,3 \tag{2}$$

$$\frac{\partial}{\partial t}\left(\rho e_0\right) + \frac{\partial}{\partial x_j}\left[\rho u_j e_0 + u_j p + q_j - u_i \tau_{ij}\right] = 0 \tag{3}$$

$\rho = fluid\ density$ $\quad t = time$ $\quad e_0 = total\ energy$

$u = flow\ velocity\ vector\ field$ $\quad p = pressure$ $\quad q = heat\ flux$

$\delta = shear\ stress$ $\quad \tau = shear\ stress$

The continuity equation (1) represents the principle of conservation of mass, meaning in any steady state process, the rate of mass entering a system must equal the rate of mass leaving the system. The momentum equation (2) is derived from Newton’s second law: the net external force is equivalent to the product of mass and acceleration of the fluid element. The energy equation (3) is derived from the first law of thermodynamics applied to a fluid volume. The first law of thermodynamics states that the total energy of an isolated system is constant; energy can transform, but cannot be created or destroyed.

The governing Navier-Stokes equations must be discretized, or reformed, in order to be applied to solve the fluid flow scenario. Several discretization methods are used by CFD software to do so. Discretization is used to reduce the partial differential equations to a set of algebraic equations. In many versions of CFD software, and in the software used in this report, a finite element (FEM) discretization method is used.

When simulating turbulent flows, which represent most flows of interest, several turbulence models are available in CFD software and the correct application of these models is critical to generating an accurate solution. Extensive research and sensitivity studies have been performed on the impact of the turbulence model on the accuracy of CFD solutions. For example, the influence of the turbulence model on accuracy for simulation of wind turbine wakes [20], for improving indoor air quality [21], and of gas and liquid pool fires [22].

It is possible to solve a turbulent flow scenario without a turbulence model, and this is referred to as direct numerical simulation (DNS). DNS requires an extremely fine grid resolution, which leads to unreasonable calculations and vast computational power [21]. A commonly used method to describe turbulent flows is defined by the Reynolds-averaged Navier-Stokes (RANS) equations, which are a time averaged version of the Navier-Stokes equations. Unsteady, or non-stationary, flows can also be solved with a RANS approach, sometimes referred to as a URANS (unsteady Reynolds-averaged Navier Stokes equations) approach. Within the RANS method, there are several turbulence models available for selection, commonly two equation models such as the k-epsilon (k-ε) and k-omega (k-ω) models. Large eddy simulation (LES) is another common mathematical model for describing turbulent flows, which reduces the computational cost of the solution by ignoring small scale regions of the flow.

CFD software is a widely used tool in the field of wind engineering in order to simulate the flow of air around a volume and evaluate the parameter of interest. As previously mentioned, many of these CFD studies are often coupled with a wind tunnel study. For example, CFD techniques used to evaluate off-shore wind turbine installations [23], in pedestrian comfort analyses [24], performance of natural ventilation systems [25], and analysis of pollutant dispersion due to wind [26].

Montazeri & Blocken [19] performed a CFD simulation of wind induced pressures on a building with and without balconies. A wind tunnel validation and sensitivity analysis was performed using a steady state RANS model approach for predicting mean wind pressure distributions on windward and leeward surfaces of a medium-rise building. Results showed that steady state RANS solutions, despite its limitations, can accurately reproduce the mean wind pressure distribution on windward building facades. Average deviations from the wind tunnel measurements were 12% and 10% for the building with and without balconies, respectively. However, for oblique flow, large discrepancies were observed between the wind tunnel measurements and the CFD results on the leeward façade.

Today, many different CFD software’s are available. Each with its own advantages, drawbacks and capabilities that influence the user’s choice based on application. The software used in this project is Autodesk CFD 2016, which is available for download free of charge. Autodesk CFD has many features which make it attractive, for example it’s ease of use and integration with 3D modelling software. However, Autodesk CFD can be seen as limited and less robust software when compared to other, more expensive programs. More advanced CFD software contains features which are not applicable or necessary for this project, such as heat transfer, solid body motion capabilities and compressible flow [27]. For the purposes of this project, Autodesk CFD is sufficient to perform the required analysis with acceptable accuracy.

As the performance of CFD techniques continue to be evaluated with validation studies such as previously mentioned, CFD simulation will quickly become a reliable and accurate method to represent and analyze fluid flows. One of the primary goals of this paper is to establish an accurate CFD model, using a wind tunnel validation study, that can be used to evaluate wind induced pressures on the Shangri-La Hotel in Toronto.

2.5 Summary

The literature review presents research on the impact of wind induced pressures on the failure of materials and objects in the environment. The mechanisms behind glass failure was explored, specifically the impact of embedded impurities on the failure of tempered glass. It was found that the failure strength of tempered glass (without imperfections) is in the order of magnitude of mega pascals (MPa) [9]. Finally, the theory and methodology of wind tunnel testing and CFD software was presented.

The conducted research provided important information and theory, helpful in the completion of experimental procedures, computer simulation, and analysis of results undertaken in this paper. Section 3 presents background information on balcony guard failures in Toronto, specifically at the Shangri-La Hotel. The wind pressure distribution on the Shangri-La Hotel was determined using an CFD model, validated by a wind tunnel study.

3. Background

The impact of wind on tall buildings is an important consideration for various reasons, as discussed in Section 2.1. Balconies on high rise buildings, especially condominiums, are a very desirable feature in today's market. However, these additions to the façade pose many challenges for designers and engineers and creating new considerations that must be taken into account. These issues are primarily related to structure and safety, but also building performance and energy use issues such as thermal bridging. Balconies completely alter the structure and façade of the building which changes the way it interacts with its surrounding environment, in particular the local wind conditions. Balconies introduce multiple areas of flow separation and recirculation across the façade, leading to very strong changes in wind pressure distribution [19]. This effect must be analyzed and assessed for occupant safety, comfort and structural issues.

3.1 Balcony Guard Failures in Toronto

In the past decade, Toronto's skyline has changed dramatically and rapidly with the addition of many new high rises. Toronto has the most high-rises under construction in North America, and has more than twice as many tall towers under construction as the second place city, New York [28]. The population of Toronto's downtown core has doubled from 1976 to 2011, and is expected to double again by 2041 [12]. In some cases, this sudden acceleration in the construction of buildings has caused a poor workmanship, and has led to building problems being overlooked. It is difficult for local building codes and standards to maintain relevance during booms in the construction industry. As new building challenges and problems arise, codes and standards must continue to develop.

Toronto's balcony guard failures, gained the media's attention in the summer of 2011. In this summer alone failures occurred in at least four separate condominiums, the Murano Towers (North and South), Festival Tower and One Bedford, when glass infill panels spontaneously shattered, falling to the streets below. The concerning trend sparked movements by industry leaders to perform investigations and begin the process of amending building code and standards. The City of Toronto and the Ministry of Municipal Affairs and Housing established an Expert Panel on Glass Panels in Balcony Guards. According to this panel, there were approximately 30 incidents of glass guard breakage during 2010 and 2011 on 11 different buildings in Toronto [29].

The report generated by the expert panel in 2012 led to the creation of a supplementary standard SB-13 in the Ontario Building Code (OBC) called “Glass in Guards,” which took effect in July 2012. SB-13 intends to: reduce the probability of breakage of glass panels and injury to persons in the vicinity of a building as a result of falling broken glass [30]. The standard specifies the types of glass to be used in balcony guards in new construction. All glass used in balcony guards must be safety glass and adhere to the following:

Table 1: Selection of glass in a guard (OBC Supplementary Standard SB-13, 2012)

Location of Glass in Guard	Type of Glass Required
Glass located beyond the edge of a floor or within 50 mm of the edge of a floor	Heat strengthened laminated glass
Glass located more than 50 mm inward from the edge of a floor	Heat strengthened laminated glass
	Heat soaked tempered glass
Glass located more than 150 mm inward from the edge of a floor	Heat strengthened laminated glass
	Heat soaked tempered glass
	Tempered glass not more than 6 mm thick

Prior to the introduction of SB-13 to the OBC, there was no specific code or standard that applied to glass balcony guards. Architects and engineers were forced to rely on general building code, not specific to balconies, which was often misinterpreted and misused. When considering the forces and loading experienced by the balcony guards, different approaches were taken, unique to the design team. Some considered only the guard loads, some considered guard loads and wind loads, but separately, and others considered the combination of both guard loads and wind loads [31].

SB-13 is only a temporary solution however and only applies to glass guards in Ontario. A more complete Canadian Standard has been drafted (CSA A500) and reviewed, which addresses all types and aspects of building guards. However, this does not address the fact that all existing balcony guards (built before July 2012) in Toronto are at risk of failing. Since 2011, there have been failures in every subsequent year on high rises such as the Four Seasons Hotel, Trump Tower, and most notably, the Shangri-La Hotel which had four failures alone.

Many possible causes and explanations for these balcony guard failures exist, and in most cases it is likely a result of a combination of these factors. One theory involves the inclusion of microscopic nickel sulphide impurities in the glass panels, which was explained in depth in

Section 2.2. Evidence of this phenomenon was found during investigations performed as a part of the 2012 Expert Panel on Glass Panels in Balcony Guards. Two consulting firms in Toronto, GRG Building Consultants and BVDA Façade Engineering, identified these impurities as the probable glass failure mechanism [29].

3.2 Balcony Guard Failures at The Shangri-La Hotel

The Shangri-La Hotel in downtown Toronto has been chosen as a case study for the purposes of this project. The building is located on the Northwest corner of Adelaide Street West and University Avenue (Figure 1). It is divided into condominium units on the upper floors and the hotel section occupies the lower portion of the building. The building is 66 floors, has a roof height of approximately 214 meters, making it the eleventh tallest building in Toronto.

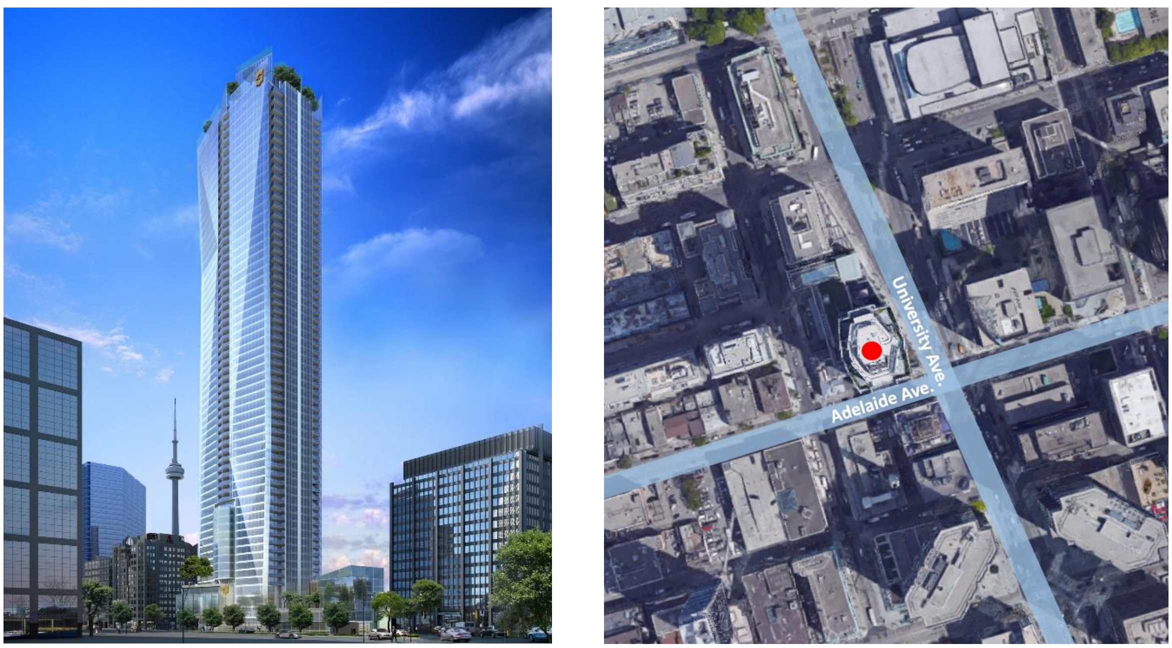

A *B*

Figure 1: The Shangri-La Hotel, rendering (A), location (B)

On each floor, there are six different balcony sections; one on each corner and one larger balcony in the center of both the East and West facades, shared by two units. As previously mentioned, four known balcony guard failures have occurred at this building since its completion in July 2012. Two of them occurred on the East façade, and two on the South façade. It is understood that the balcony guards are constructed with tempered glass.

The exact pane of glass that failed could be determined for two out of the four failures from various news sources, such as the images in Figure 2 from the Toronto Star (A) and the Globe and Mail (B).

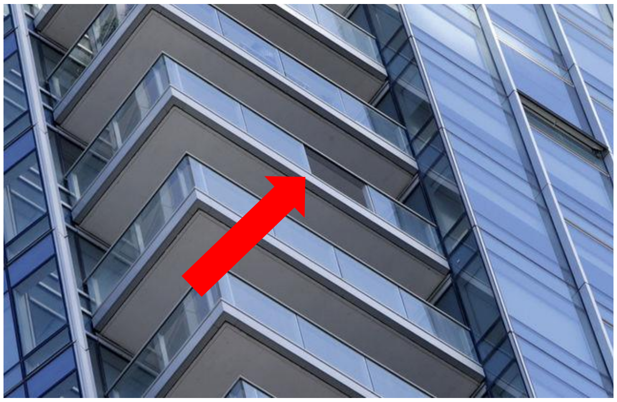

A: Toronto Star (2013) B: Globe & Mail (2013)

Figure 2: Failure location photographs

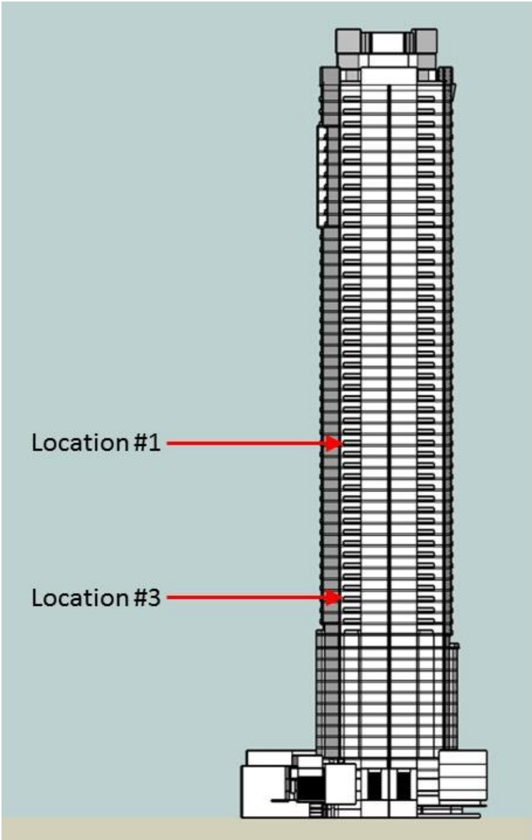

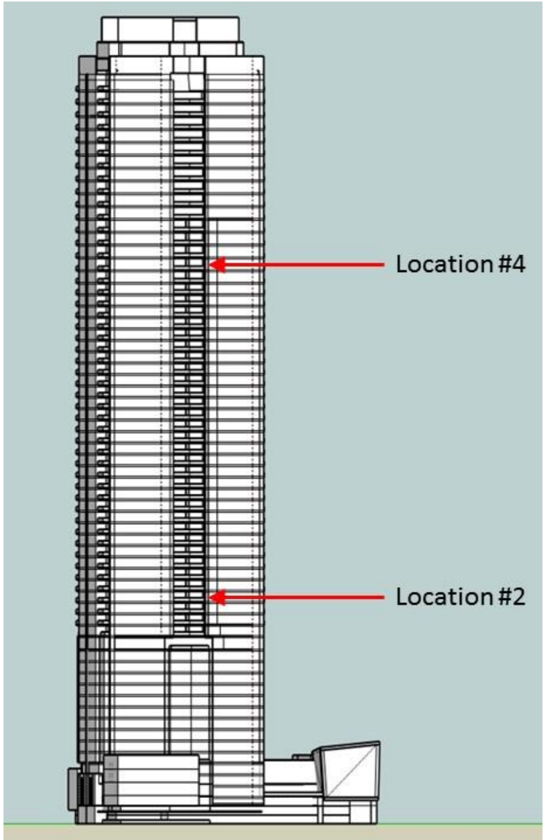

A B

Figure 3: Failure locations, South elevation (A), East elevation (B)

Table 2: Failure location information

	Location 1	Location 2	Location 3	Location 4
Date of failure	Jan. 23, 2013	Sept. 10, 2013	Nov. 24, 2013	July 17, 2014
Floor/Facade	37/South	23/East	23/South	51/East
Exact Location	Unknown	Known	Known	Unknown
Approx. Height (m)	102	60	60	144

4. Methodology

The objective of this methodology is to analyze the effect of local wind conditions on the Shangri-La Hotel's balcony guards using CFD software. In order to do this, an accurate and reliable external flow CFD model must be developed, which will be used to calculate the wind pressure distribution of the entire façade.

Validation of the CFD methodology used in this analysis will be performed with a wind tunnel study of a simple building model with four balconies. Experimental data was obtained over 16 pressure taps built into the balconies of the wind tunnel model. The wind tunnel model geometry and environment was replicated in CFD software, and the data obtained from the wind tunnel testing was compared with the CFD results through a sensitivity analysis of the software's parameters and settings. Ideally, a scale model of the Shangri-La Hotel would be tested in the wind tunnel for CFD validation, however this was not possible due to scale and model complexity issues. In addition, accurate representation of approaching flow would not be achievable with the limited resources and capabilities of the available wind tunnel. If the software and approach can be validated in this simple way, it can be applied on a full-scale model and produce accurate results.

With the results of the validation study, a full-scale CFD model of the Shangri-La Hotel and its surrounding buildings was developed. In order to accurately represent the local wind conditions, a historical wind analysis was performed using weather data from Toronto's Billy Bishop Airport. Average wind conditions and gust conditions (wind direction and speed) were identified and applied to the CFD simulation. The results from the CFD simulation were used to obtain surface pressures at the failure locations for the various wind conditions. The CFD simulation results were also used to identify areas of the façade that are of concern and should be monitored.

5. Validation Study

5.1 Wind Tunnel Study

5.1.1 Scaling

The intention of this study is not to simulate a real life scenario or environment, but is a means of assessing and exploring the software's settings and parameters to see how they affect the accuracy of the solution. Therefore, scaling of the model geometry and parameters such as wind speed is irrelevant, however the theory and methodology is discussed below.

In order to replicate a real scenario and condition, scaling must be applied to the wind tunnel flow, model and data collection parameters. The velocity scale (λ_V) is determined by the capabilities (range of flow speed) of the wind tunnel in question. For example, if the wind tunnel is limited to speeds of 20 m/s and the design wind speed of the building in question is 60 m/s, then the velocity scale would be 1:3. The length scale (λ_L) relates the size of the real building to the size of the model. The length scale is dictated by the depth of the simulated boundary layer [32], the characteristics of the flow generated by the wind tunnel [17], by the physical limitations of the wind tunnel test section, and the desired blockage ratio. Since aspects of both time and space are scaled in the wind tunnel testing, the data acquisition also occurs at a scaled rate. For example, if the time scale is 1:100, a wind tunnel sampling rate of 400 Hz corresponds to 4 Hz (4 samples per second).

The time scale (λ_T) is related to the other two scales and is defined as [17]:

$$\lambda_T = \frac{\lambda_L}{\lambda_V} \tag{4}$$

5.1.2 Equipment and Data Acquisition

The wind tunnel used in this experimental study is a closed circuit wind tunnel, powered by a 50 horsepower [HP] 'Axivane' fan. The test section base has dimensions of 0.415 m (width) by 1.58 m (length), and inlet dimensions of approximately 0.4 m by 0.4 m. See Appendix for additional specifications.

A

B

Figure 4: Wind tunnel, open (A), closed (B)

The pressure transducer used in the experimental data collection was a 16 channel Scanivalve unit (DSA3217/16Px). Network connection to a local computer allows its settings it to be controlled by the program ScanTel. The reference port was used appropriately in each test to measure the desired reference pressure. The parameters used to define the method of data collection are: period, average, frames per scan and sampling rate. The period (specified in micro-seconds) is the amount of time between samples. Average defines the amount of samples taken before the software produces an averaged output. For the purposes of this analysis, the average was set to 1 because the raw data was analyzed using Microsoft Excel. Frames per scan (FPS) is the amount of samples taken, after which point the data collection stops automatically.

The data acquisition in a test such as this is controlled by the sampling rate, which represents the number of samples taken per second (Hz). The maximum sampling rate is inversely proportional to the number of inputs on each pressure transducer and the period. The sampling rate for pressure measurements is typically between 300 and 500 samples per second per input (Hz/input) [17].

$$Sampling\ Rate = \frac{1}{\#\ of\ inputs \times Period \times Average} \tag{5}$$

The equipment’s minimum period of 125 µs produced a sampling rate of 500 Hz which was too fast for the computer system to process. Therefore, the period was increased to 150 µs which resulted in an acceptable sampling rate of:

$$Sampling\ Rate = \frac{1}{16 \times Period \times Average} = \frac{1}{(16)(0.000150\ s)(1)} = 417\ Hz$$

The total amount of measurements taken depends on the chosen sampling time. For low-speed pressure measurement applications the sampling time is typically between 30 and 60 seconds [17]. With the sampling rate limited to 417 Hz, the frames per scan (FPS) was selected to produce an acceptable sampling time of 60 seconds.

$$Sample\ time = \frac{FPS}{Data\ Rate} \tag{6}$$

$$FPS = (Data\ Rate) * (Sample\ Time) = (417\ Hz)(60\ s) \approx 25{,}000$$

Based on the recommendations, the following settings and parameters were selected and calculated (Table 3).

Table 3: Data acquisition settings

Setting	Value
Period (μs)	150
Average (AVG)	1
Frames per Scan (FPS)	25,000
Sampling Rate (Hz)	416.67
Sampling Time (s)	60

5.1.3 Wind Tunnel Calibration

The wind tunnel was controlled by a variable speed remote. The user may input a desired frequency, which correlates to a certain wind velocity in the wind tunnel test section. The correlation between input frequency and wind velocity was determined before any tests could take place. Calibration would also allow for the determination of the test section conditions (pressures) at various speeds, which are necessary for data analysis.

Common practice in wind tunnel studies is to simultaneously measure the test section pressures while testing the model using instrumentation such as a pitot tube. Often this is not possible due to limited space in the test section and instrumentation interference with the model. Therefore, another approach is taken, using a pitot tube and an empty test section to determine two calibration constants, K_p and K_q. Once these calibration constants are determined at various wind speeds, they can be used to analyze data when it is not possible to directly measure test section pressures (ie. when the model is mounted in the test section).

$P_{C1} = contraction\ inlet\ static\ pressure$

$P_{C2} = contraction\ outlet\ static\ pressure$

$P_t = test\ section\ total\ pressure$

$P_s = test\ section\ static\ pressure$

$P_d = test\ section\ dynamic\ pressure$

$P_i = measured\ pressure$

$\rho = test\ section\ static\ air\ density$

$U = test\ section\ wind\ speed\ (m/s)$

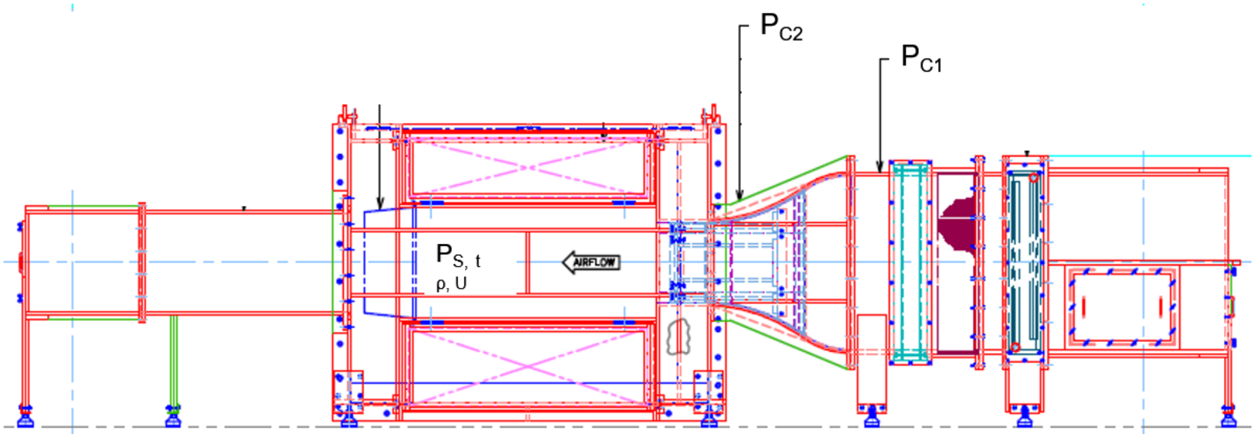

Figure 5: Location of calibration pressure measurements

Test section pressures are related as such:

$$P_t = P_d + P_s \tag{7}$$

Where, dynamic pressure is related to the kinetic energy of the fluid:

$$P_d = 0.5\rho U^2 \tag{8}$$

Therefore, the test section wind speed is calculated using the following relation:

$$U = \sqrt{\frac{2P_d}{\rho}} = \sqrt{\frac{2(P_t - P_s)}{\rho}} \tag{9}$$

Test section total pressure (P_t) and static pressure (P_s) are measured using a pitot tube mounted in the wind tunnel.

And the calibration constants are defined as:

$$k_p = \frac{P_s - P_{C2}}{P_{C1} - P_{C2}} \qquad k_p = \frac{P_t - P_s}{P_{C1} - P_{C2}} \qquad (10), (11)$$

Six different input frequencies were tested (6, 10, 15, 20, 25 and 30 Hz) in three different trials and the following averaged results were obtained.

Table 4: Calibration constants for tested input frequencies

Input Frequency (Hz)	K_q	K_p	U (m/s)
6	0.93788	0.10584	5.52
10	0.92537	0.10659	9.48
15	0.92055	0.10810	14.45
20	0.91639	0.11074	19.46
25	0.91135	0.11497	24.36
30	0.90661	0.11962	29.28

In order to compare the wind tunnel results with the CFD results, the mean pressure coefficient had to be determined. The general definition of the pressure coefficient is:

$$C_p = \frac{P_i - P_s}{P_d} \tag{12}$$

As mentioned, since it is not possible to measure the test section static pressure (P_s) during the test, this formula must be expressed in terms of the calibration coefficients which were previously determined:

$$C_p = \frac{\left(\frac{P_i - P_{C2}}{P_{C1} - P_{C2}}\right) - k_p}{k_q} \tag{13}$$

Where P_i is the mean of the 25,000 pressure measurements taken on each balcony face.

5.1.4 Wind Tunnel Model

The model that was created is shown below in Figure 6. It consists of three buildings of varying sizes, as simplified masses, constructed with 0.75 inch medium-density fiberboard (MDF). The middle building has one balcony on each façade (total of 4), where the pressure measurements were taken.

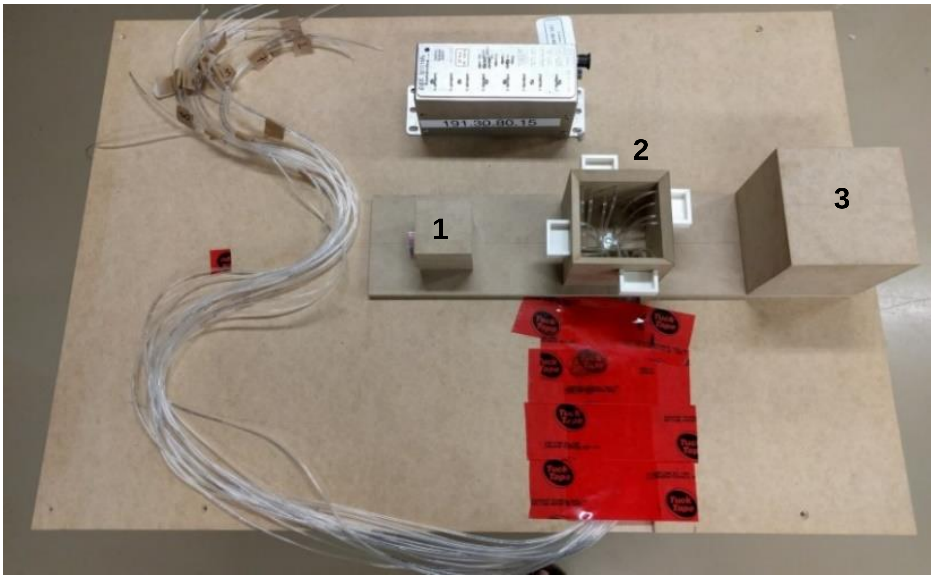

Figure 6: Wind tunnel model with pneumatic connections

A base was constructed that would be used to mount the model in the wind tunnel and allowed for the rearranging of the three buildings and for their rotation to test three different angles of attack (0°, 10°, 20°). Intentions were to test two configurations at the three angles of attack: one with the small building upwind from the test building, and one configuration with the large building upwind from the test building. However, unforeseen limitations in the construction process only allowed for the testing of the configuration shown in Figure 7, at all three angles of attack.

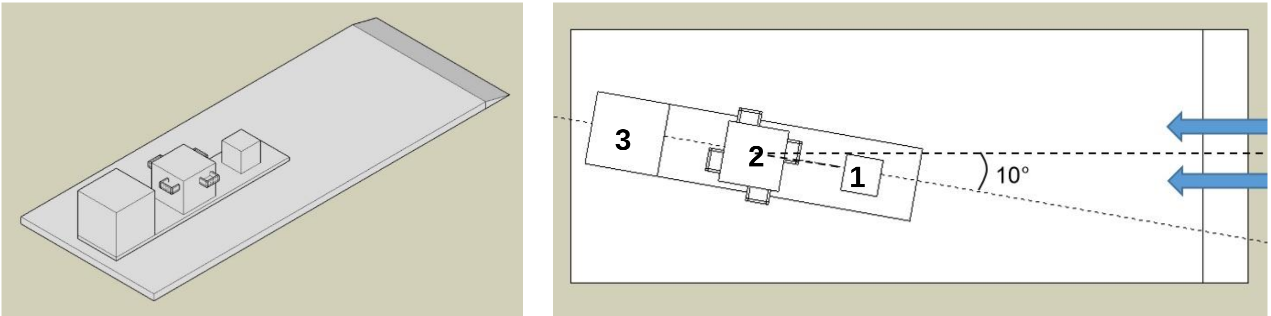

A *Bn*

Figure 7: Sketchup representation, 0° orientation (A), 10° orientation (B)

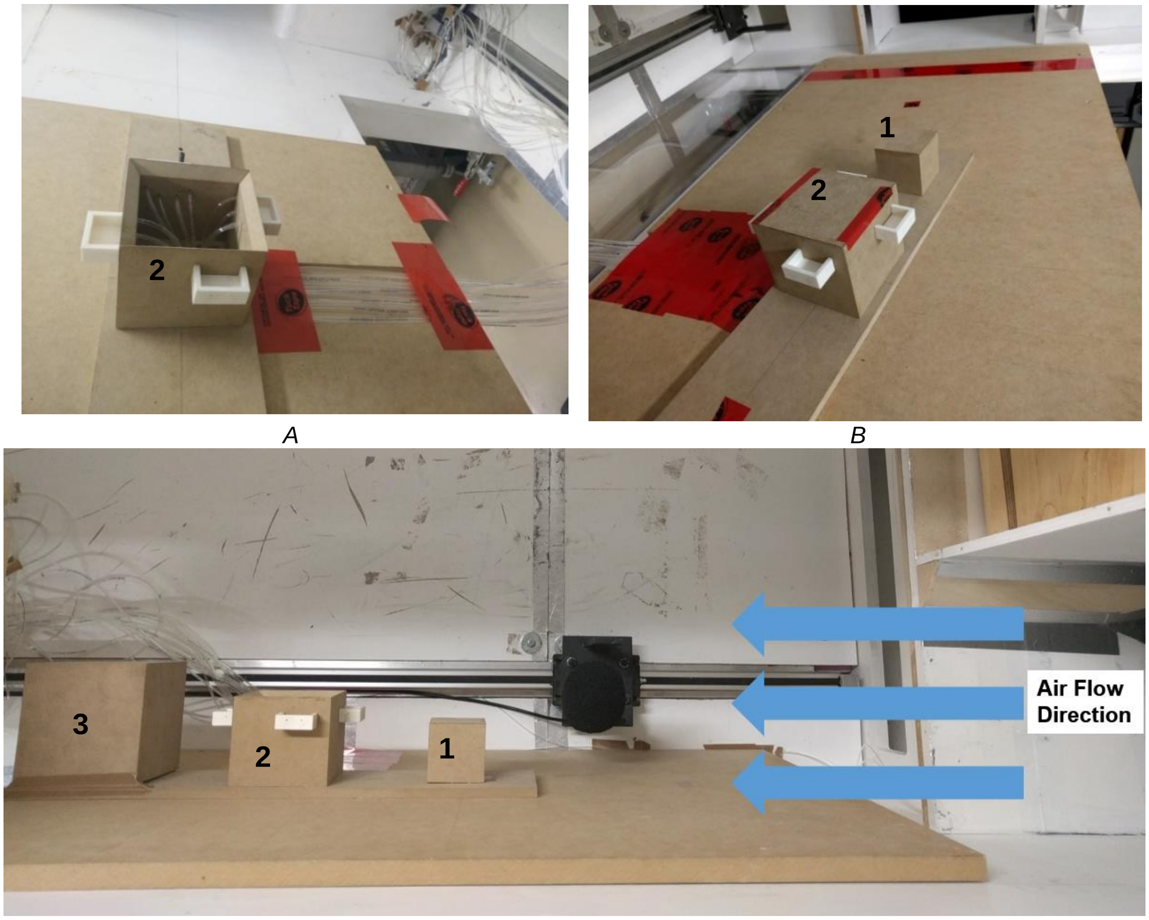

Figure 8: Mounted wind tunnel model (C)

As discussed in Section 2, the blockage effect of the model on the wind tunnel flow must be minimized or taken into account in the data analysis. The cross sectional area of the wind tunnel test section inlet is 0.17 m^2. In order to maintain an acceptable blockage ratio of under 15% [15], the model must account for a maximum of 0.0255 m^2 (255 cm^2) during all test scenarios. The following dimensions were chosen for each building, and the resulting blockage ratios for each test orientation are shown in Table 5. Note that the 20° orientation has a blockage ratio of 18%. The effect of the high blockage ratio is discussed as a source of error for this orientation.

Table 5: Model dimensions and blockage ratio

Building	Length (cm)	Width (cm)	Height (cm)
1	6	6	6
2	10	10	9
3	12	12	12

Orientation	Projected Area (m^2)	Blockage Ratio
0°	0.0162	9.5%
10°	0.022	12.9%
20°	0.0306	18%

To obtain the desired pressure measurements on the exterior surfaces of the balcony, a physical connection had to be established between the balcony surfaces and the Scanivalve tubes. The ideal way to accomplish this would be to construct holes that run from the balcony surface and through the interior of the balconies to allow the tubes to connect on the inside of the building. This ensures that the tubes are not obstructing the flow and are all on the interior of the model which best represents the situation. Due to the small, detailed geometry of the balconies, they were 3D printed using ABS plastic and geometry as shown in Figure 9.

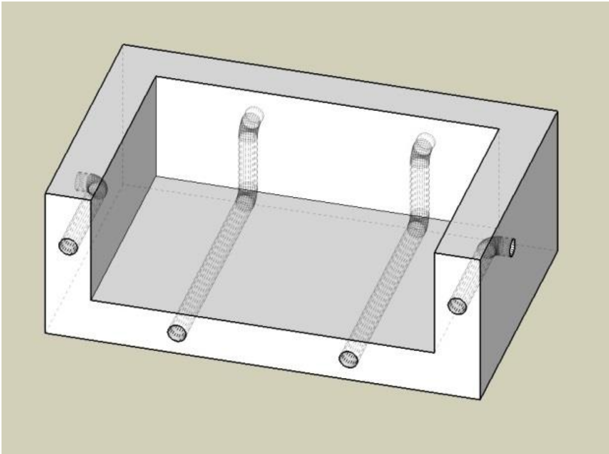

Figure 9: Model balcony geometry

Four measurement locations were created on each balcony as shown in Figure 10, for a total of 15 measurement points. Note that measurement point 1 was discarded due to limited available ports (16) and the requirement to measure the wind tunnel contraction inlet pressure (P_{C1}). The connection between the balcony edges at the pressure transducer was made with 1/16" (ID) pneumatic tubing.

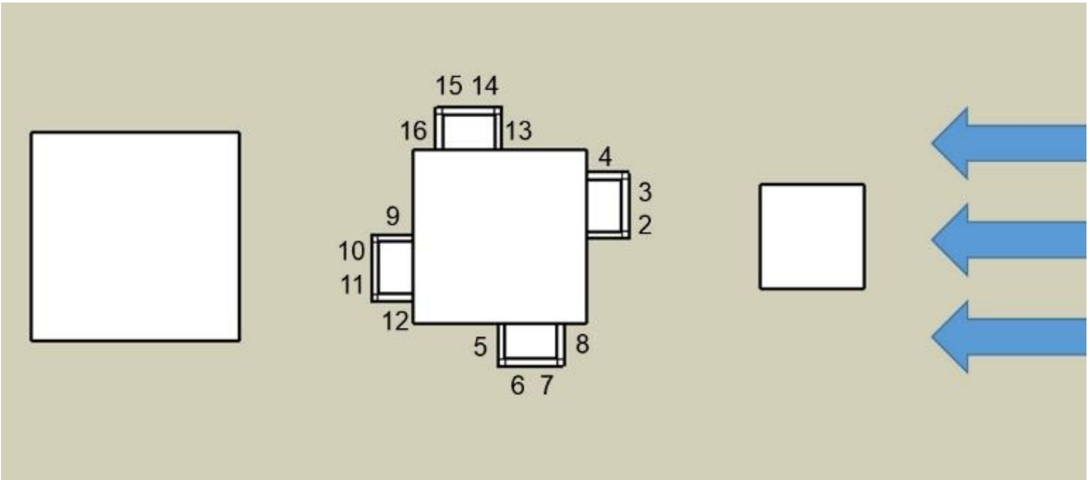

Figure 10: Pressure tap locations

5.1.5 Results

The 25,000 data points taken at each measurement location over the sample time of 60 seconds were statistically analyzed. The maximum, minimum and mean pressure at each measurement location was calculated. The standard deviation (σ) of the data collected at each location was calculated as the square of the variance:

$$Variance = \sigma^2 = \langle (P_i - P_{mean})^2 \rangle \tag{14}$$

It was found that the measurement locations had varying values of standard deviation (Figure 11). For example, in the 0° orientation at 20Hz, the standard deviation ranged from 3.6 Pa (location 8) to 48.7 Pa (location 4). The two graphs below show the statistical analysis of these two measurement points.

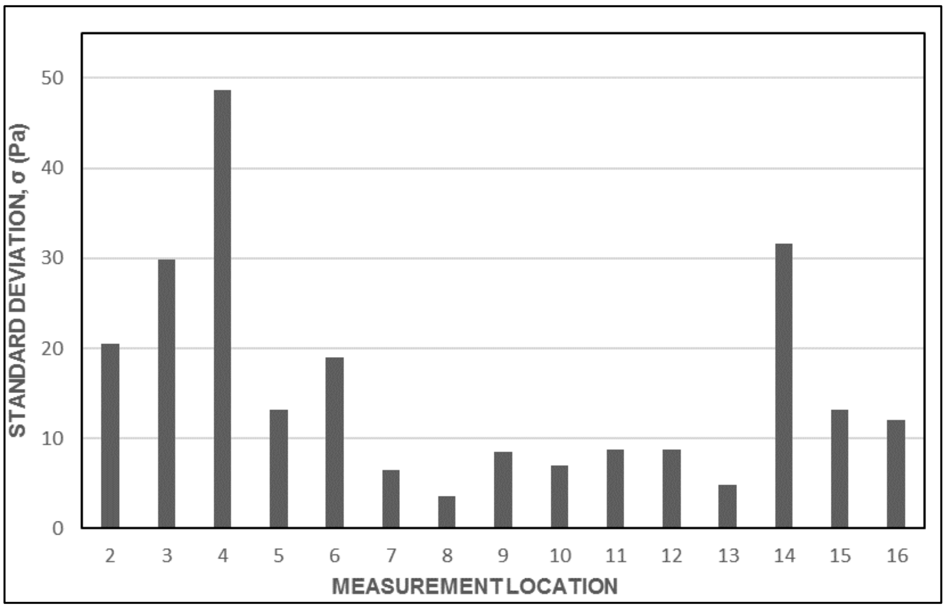

Figure 11: Standard deviation, all measurement locations, 0° orientation at 20 Hz

As can be seen in Figure 12, measurement location 4 displays quite a wide range of data recorded in the sampling period, while measurement location 8 (Figure 13) displays a much more evenly distributed range of collected data. Measurement locations with high degrees of variance from the mean (standard deviation) for the 0° orientation include 3, 4 and 14. Wind pressure measurements often produce data with a wide degree of variation, since wind (especially at high speeds) produces such an unsteady, dynamic and turbulent force on a given surface. High degrees of variation could also be due to other experimental errors such as hole blockage or other connection issues between the pressure taps and the equipment. Sources of error are discussed in Section 5.2.

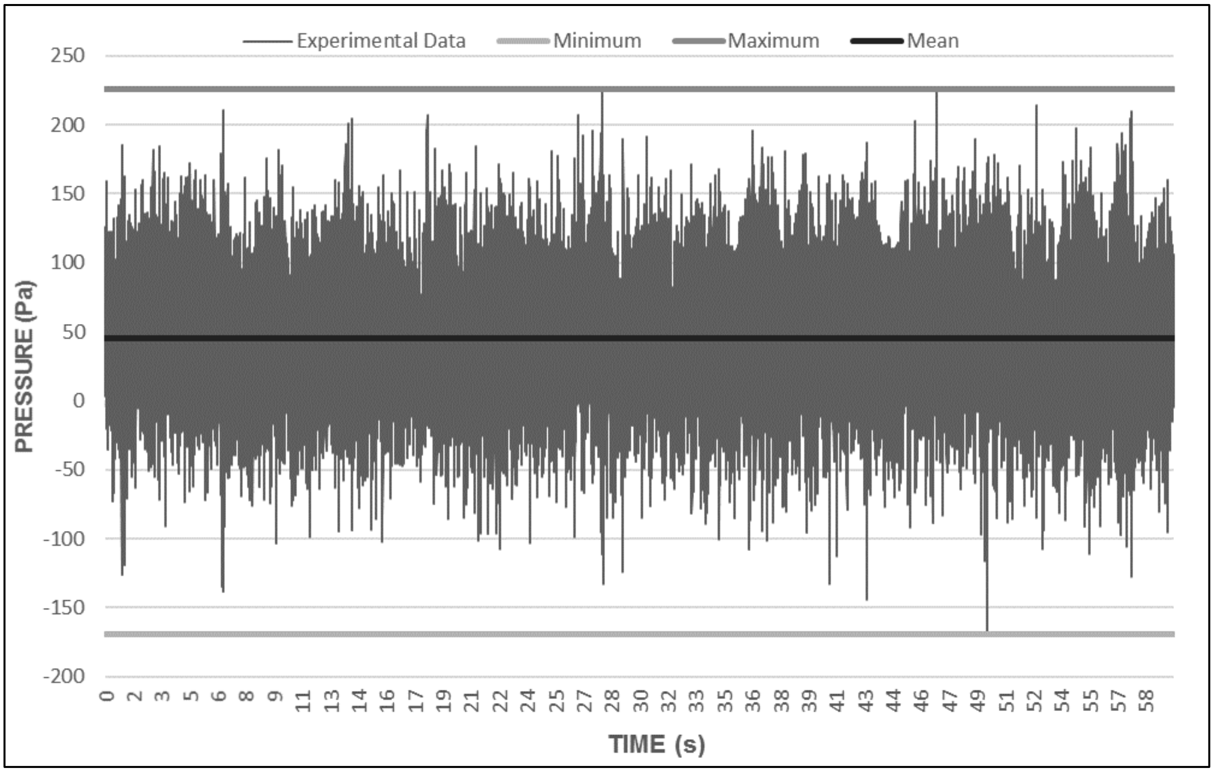

Figure 12: Measurement location 4 experimental data

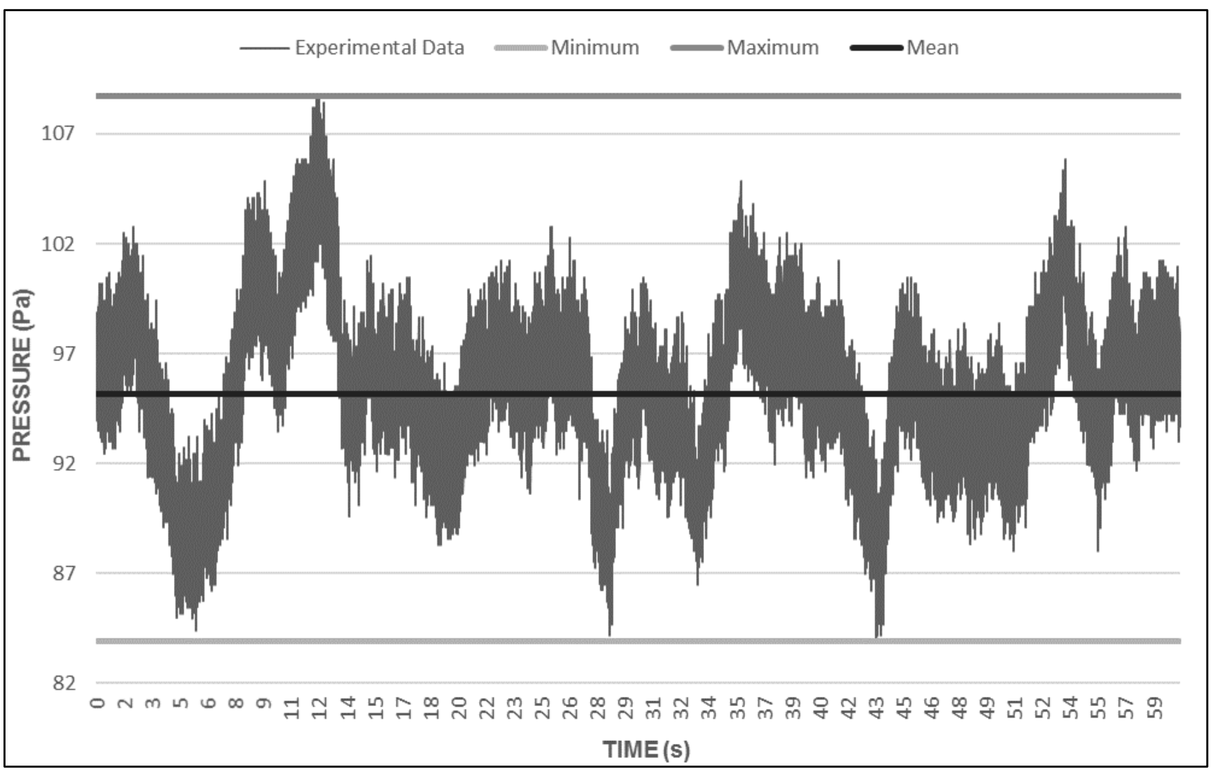

Figure 13: Measurement location 8 experimental data

In order to complete the validation study, experimental results from the wind tunnel must be compared to the CFD simulation results. From the experimental results it was determined that for some measurement locations, a high degree of variation exists in the dataset. The variation poses a challenge in determining what values (maximum, minimum, mean or other) should be compared to the simulated results. The measurement feature used in the CFD software calculates the average pressure on the surface of interest. Therefore, it is assumed that the experimental and simulated mean pressure coefficient values are to be compared. A summary of the 0° orientation wind tunnel experimental data for each measurement location is shown in Figure 14 below.

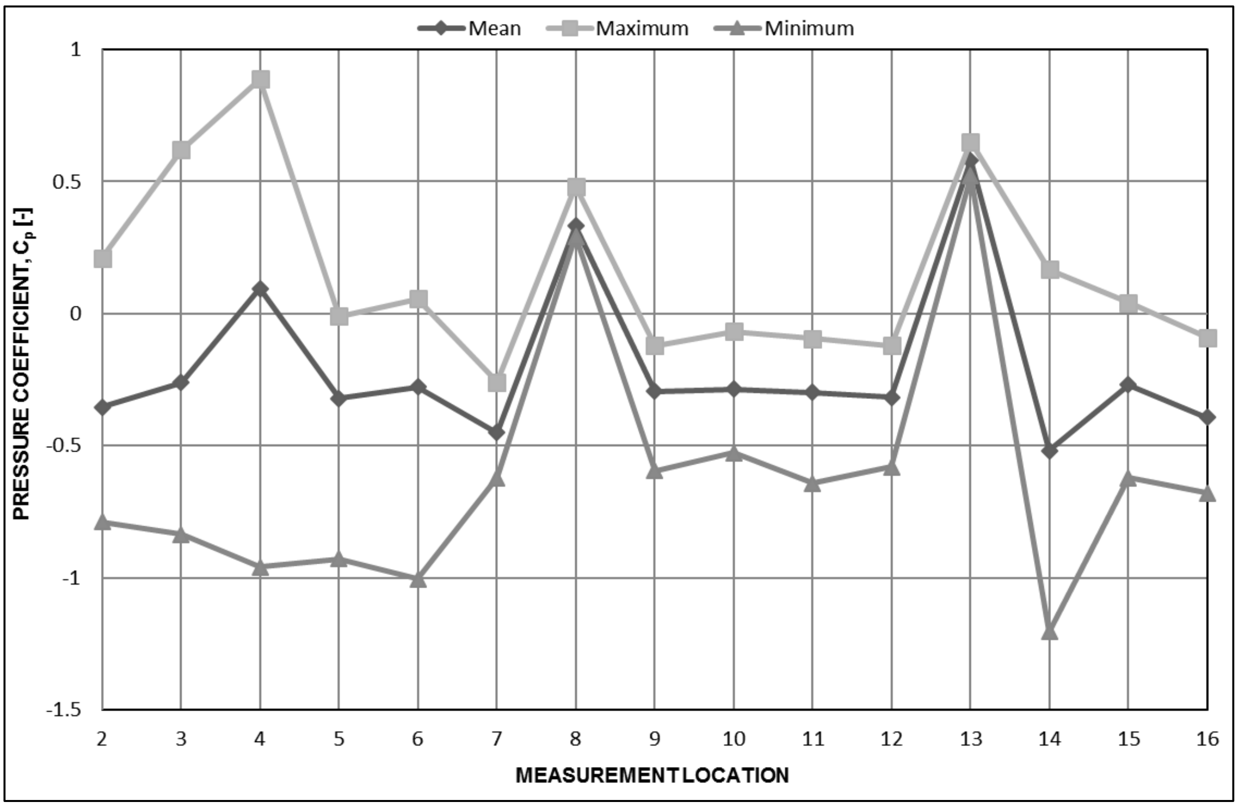

Figure 14: Wind tunnel experimental results, 0° orientation at 20 Hz

Results and collected data from all experimental trials (including 10° and 20° orientation) can be seen in the Appendix and the results are summarized in Figure 15 and Figure 16 below. It is interesting to note that the standard deviation of measurement locations 2 to 6 decreases as the model is rotated to 10° and 20° orientations.

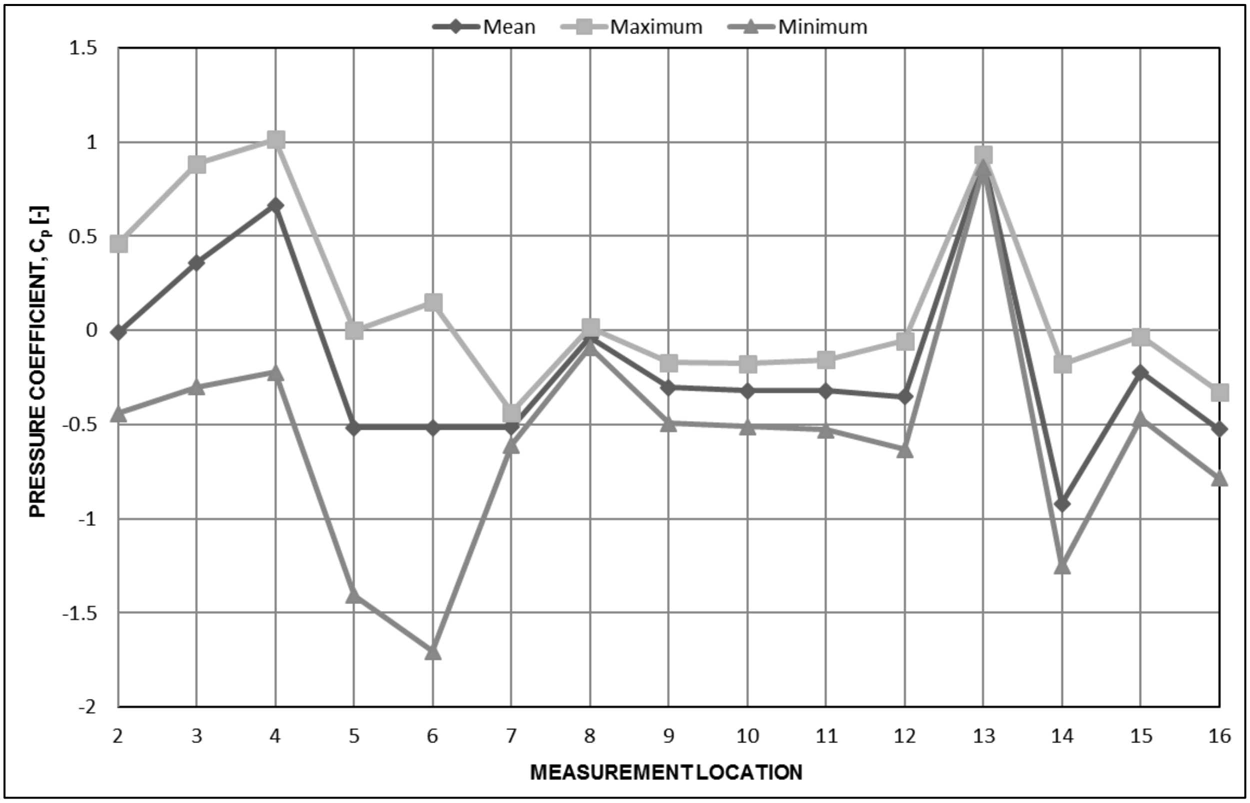

Figure 15: Wind tunnel experimental results, 10° orientation at 20 Hz

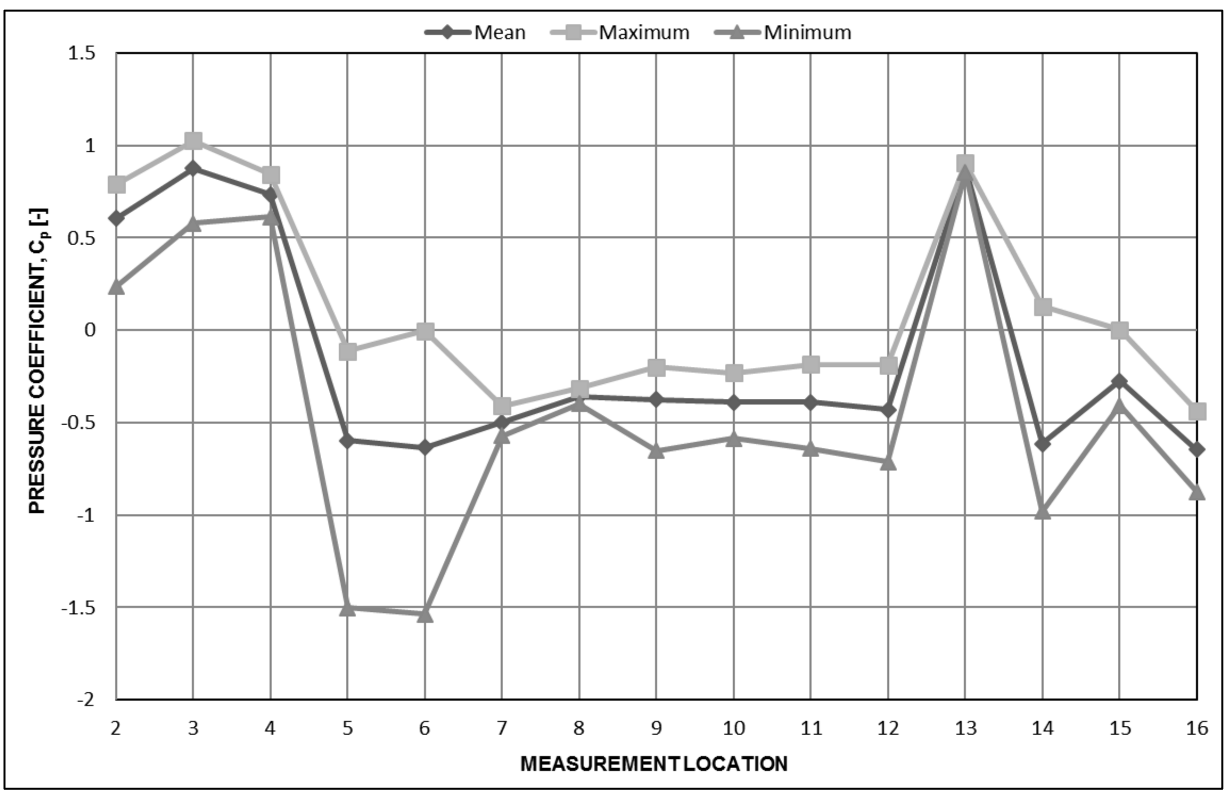

Figure 16: Wind tunnel experimental results, 20° orientation at 20 Hz

5.2 CFD Study

The wind tunnel model and scenario was modelled in CFD software and a sensitivity analysis was performed on the CFD set-up parameters and simulation settings.

5.2.1 Set-Up: Autodesk CFD

The scale model geometry was created in Sketchup and imported into Autodesk Simulation CFD. The goal was to replicate the scale model and wind tunnel conditions in the CFD software with the following set-up parameters.

In order to simulate external air flow, a volume was created which surrounded the model. The dimensions of this external volume were the same as the wind tunnel test section. Boundary conditions had to be applied to the external volume to simulate the air flow. An inlet velocity condition was specified at 19.46 m/s, an outlet pressure condition of 0 Pa (gage/static), and the base was considered as a wall. The top and sides were assigned a slip/symmetry condition which allows the air to flow along this boundary instead of being stopped, which typically occurs along a wall. The slip/symmetry condition was used at the top and side boundaries because the wind tunnel test section is in fact larger (in width and height) than the inlet. This simplified the simulation, rather than precisely modelling the entirety of the test section which contained complicated geometry and various materials.

Materials were assigned accordingly to each volume. ABS plastic was assigned to the balcony volumes, all other parts of the model were assigned the material “soft wood” to simulate the MDF, and the external volume was assigned the fluid properties of air at the test temperature (34°C) and conditions.

The following sections present the various settings and parameters considered in the sensitivity analysis that the user is able to modify in Autodesk CFD.

Meshing

In order for CFD software to simulate the movement of a fluid, the geometry must be divided into small pieces in a process called meshing. The small pieces are called elements, and the corner of each element, where the calculation is performed, is called a node. When the fluid volume is meshed in three dimensions, the elements are generally tetrahedrals. While, when a surface is meshed in two dimensions, the elements are generally triangular.

In Autodesk CFD Simulation, and most CFD software, there is a feature called Automatic Mesh Sizing. When this option is selected a mesh distribution is generated of different element sizes based on a topological analysis of the geometry which considers curvature, gradients and proximity of objects in the model. The software also allows for the manual modification of mesh distributions in any region of the model. The user to customize the mesh size (refine or coarsen) based on his or her needs.

Another useful feature of Autodesk CFD is mesh adaptation. Mesh adaptation uses solution results to automatically adapt and change the mesh to produce increasingly accurate results. When mesh adaptation is enabled the user sets the number of solution cycles to run. An initial base case solution is produced with an auto sized mesh, and the mesh is adapted in locations where the previous solution identified regions of complexity. The mesh is adapted based on this solution of the field variables (velocity, pressure and temperature) along with the optional parameters described below.

The “allow coarsening” option allows the mesh to not only refine itself in regions of flow complexity, but also become coarser and simplified in regions where refinement is not required. Enabling the “flow angularity” option improves the mesh resolution in regions that contain large amounts of circulatory flow and/or flow separation, such as convex corners. A free shear layer occurs in areas where the free stream flow meets a region of much slower flow, such as a wake or separation region. Enabling free shear allows the mesh to refine itself in these areas in order to accurately predict the flow by capturing the large velocity gradient within the shear layer. The external flow option should be enabled when free shear layers are expected in regions that are not closely bounded by walls or other objects. This is often the case in external flow simulation, such as this one, that involve a large external volume of air that surrounds the model.

In addition to the meshing of volumes and of the fluid itself, the mesh in all fluid-solid interfaces must be carefully considered. This region is called the “wall layer” or “boundary layer” and is critical for accurate flow representation. Autodesk CFD allows for the modification of the meshing in this region based on four settings: wall blending, number of layers, layer factor and layer gradation. Wall blending smoothens the transition between the wall layers and the adjacent mesh, layer factor corresponds to the overall thickness of the wall layer and layer gradation alters the growth rate of the layers. Wall layer enhancement settings must be modified for certain simulation set-ups. Figure 17 depicts a common type of enhancement of the wall layer.

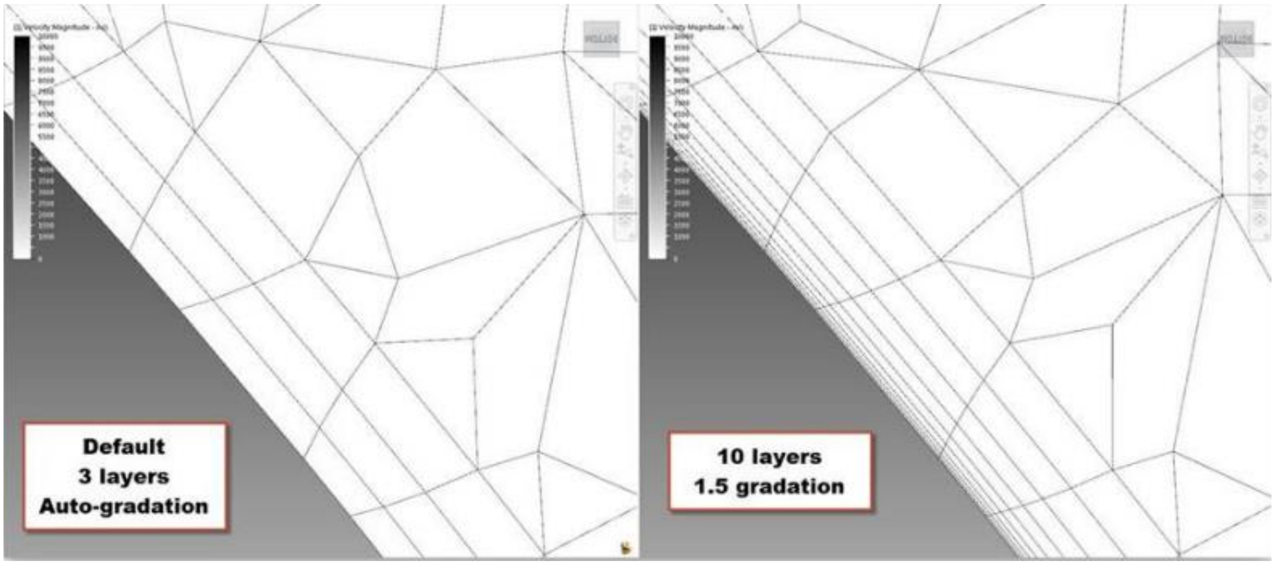

Figure 17: Wall layer mesh enhancement

Turbulence Models

For turbulent flows, such as the wind tunnel flow being simulated, Autodesk CFD gives the user the choice between several turbulence models based on the application. Turbulence models can be changed in order to improve the accuracy of the solution. A certain model should be selected based on factors such as the speed of flow, internal versus external applications and the model geometry. The software's default turbulence model is the k-epsilon (k-ε) model which is a general purpose model that performs well for various applications. An alternate turbulence model that will be explored in this paper is the Shear Stress Transport k-omega (SST k-ω) model which is recommended for external flow applications and is robust over a wide range of flow types, especially low velocity flow. SST k-ω combines two turbulence models, using of k-ε in free shear layers, and k-ω in the inner region of the boundary layer. Unlike other turbulence models, the SST k-omega model simulates turbulence all the way up to the wall, instead of using wall functions to define the flow in the wall layer. When using this turbulence model, the wall layer settings must be considered and modified in order to produce a reliable simulation and accurate solutions.

Solution Control

By default, Autodesk CFD uses an "Intelligent solution control" which automatically stops the solver when convergence is reached. This convergence is determined when the time averaged variables (velocity components – V_x, V_y, V_z, pressure, temperature) have reached a steady state condition and are not changing (to a certain tolerance) with each iteration. The user has the ability to change the convergence threshold criteria levels between “loose” and “tight,” with a default setting in-between the two (moderate). For example, in Figure 18 the convergence threshold criteria was set to “moderate” and the simulation achieved convergence after 568 iterations when the time varying functions have reached a steady state (ie. The lines flatten).

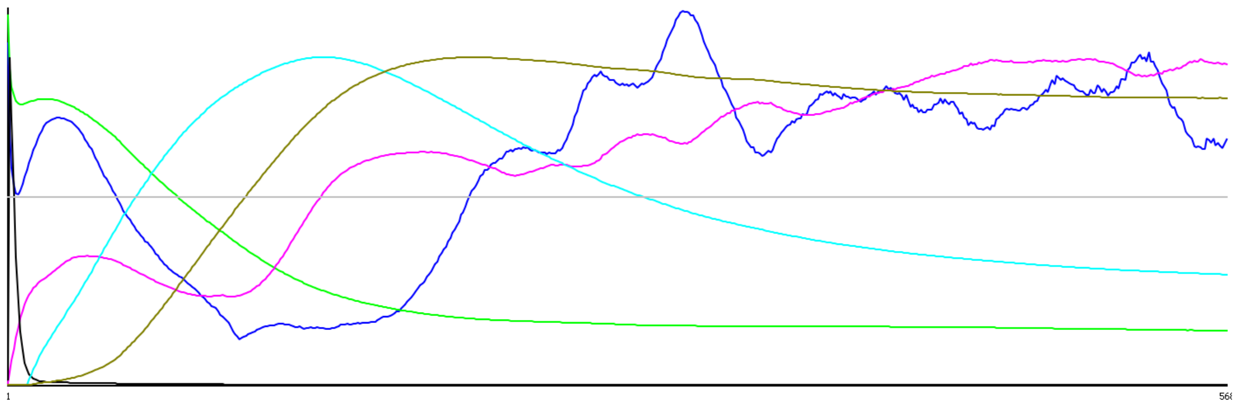

Figure 18: Autodesk CFD convergence plot example

Advection Scheme

The advection scheme controls the numerical mechanism which transports a quantity (eg. velocity or temperature) through the solution domain. The user can choose between five different advection schemes based on the application. Autodesk CFD’s default advection scheme is Monotone streamline upwind (ADV-1), which is numerically stable and recommended as a starting point for most models. An alternative advection scheme that will be explored in this paper is the Modified Petrov-Galerkin advection scheme (ADV-5). ADV-5 is less numerically stable than ADV-1, however it is recommended for use with the SST k-omega turbulence model and for external flow applications.

5.2.2 Sensitivity Analysis

The “wall calculator” feature in Autodesk CFD was used which calculates the average pressure on each exterior surface of the balcony, and the pressure coefficient was calculated. In order to determine the most accurate CFD model, these values were then compared to the experimentally determined mean pressure coefficients for various trials presented below.

As expected, the pressure coefficient values on the balcony surface are independent of flow speed and remain constant (within a small degree of error) with change in wind velocity. Therefore, for the purpose of comparison between the wind tunnel and CFD results, the 20 Hz speed (19.46 m/s) will be analyzed.

The following section presents the results for the 0º orientation. The results for the 10º and 20º orientations can be seen in the Appendix. Note that each trial does not represent the cumulative change in multiple settings, but represents the changing of a single CFD parameter or setting. The final simulation is the accumulative result of the change of all mentioned parameters.

Trial 1 – Default Settings

First, a CFD model was created which implemented the following software default settings when developing a solution.

Meshing: Automatic Sizing ("Autosize")

Table 6: Trial 1 finite element summary

	Fluid	Solid	Total
Number of Nodes	16,142	1,986	18,128
Number of Elements	58,862	15,770	74,632

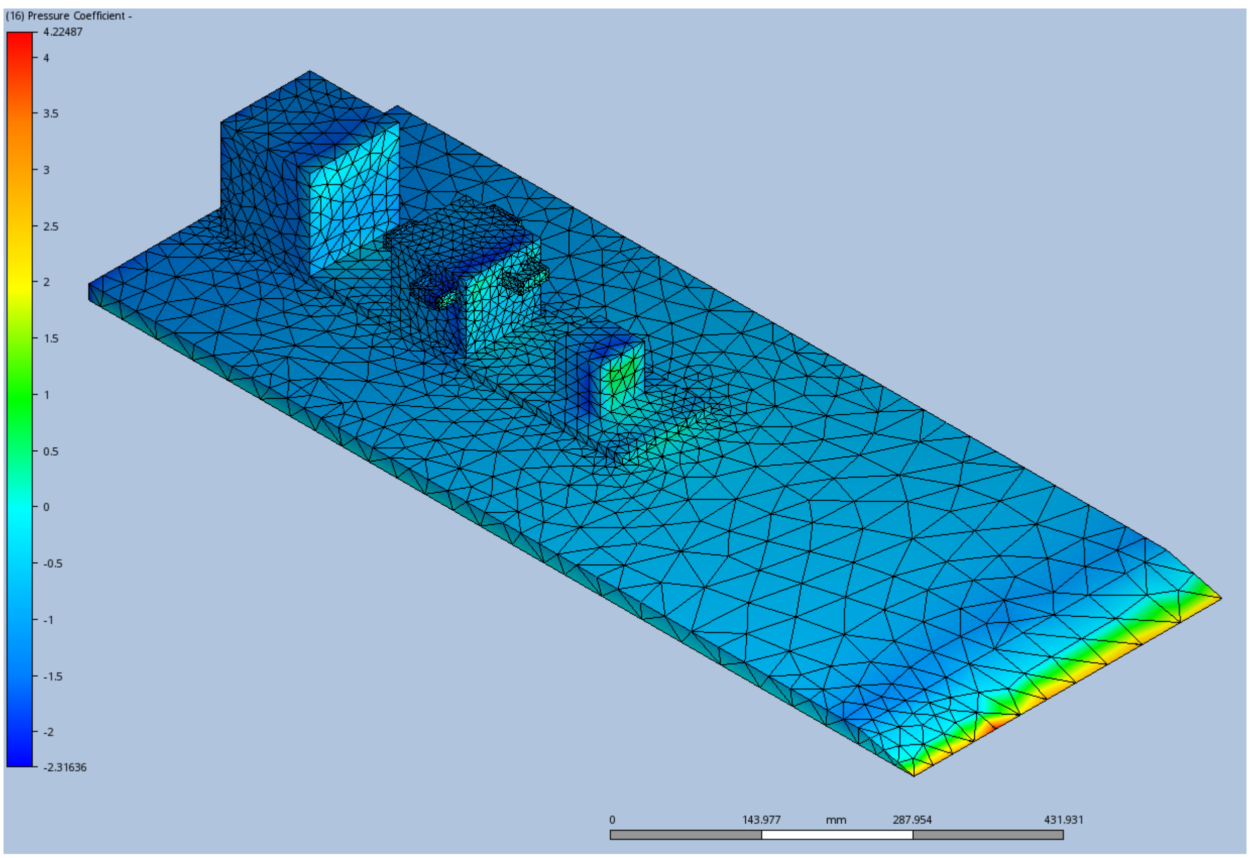

Figure 19: Trial 1 meshing and results

Wall Layer Enhancement Settings

For this trial the wall layer settings are left at their default values which are:

- Wall blending: Off
- Number of Layers: 3
- Layer Factor: 0.45
- Layer Gradation: Auto

Turbulence Model: k-epsilon

Solution Control (Convergence Threshold Criteria): Moderate

Advection Scheme: Monotone streamline upwind (ADV-1)

Number of Iterations for Solution Convergence: 335/371 (tight convergence threshold criteria)

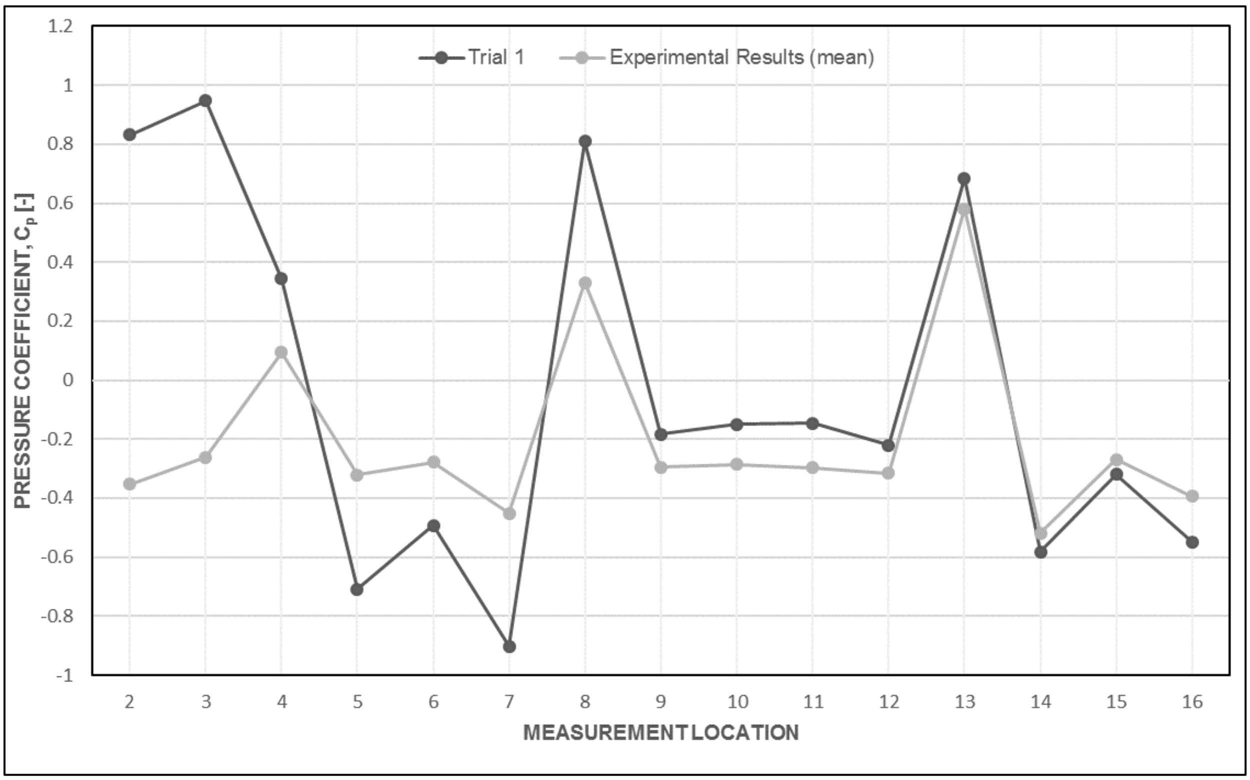

Figure 20: Trial 1 - Software default settings

As can be seen in Figure 20, the default settings in Autodesk CFD produce a solution that does not agree with the experimental wind tunnel results. Some of the general trends of the experimental result can be seen, however the overall result of the simulation does not accurately represent the experimental data. Improvements to the simulation must be explored in order to increase accuracy.

A significant deviation between the simulated result and the experimental result occurs at measurement location 2 and 3. For example, at location 3, the experimental data results in a negative pressure coefficient (or suction) of -0.35 while the simulation produces a positive pressure coefficient of 0.84. This amount of deviation suggests that an experimental error had occurred in these locations, such as blockage of the pressure tap hole, or that the CFD simulation set-up was so inaccurate that it produces a deviation of this scale. Measurement locations 2 and 3 were the closest in location to the small building upwind from the measurement locations. In this critical region, behind the leading building, the wake must be accurately represented by the software in order to produce accurate results at measurement locations 2 and 3. In order to do this, the meshing in this region should be carefully considered, and further analysis of the physics of the flow in this situation should be analyzed.

Simulation results at several measurement locations are quite agreeable with the experimental results, in particular measurement locations 13, 14 and 15, which display absolute differences in pressure coefficient of less than 0.1.

The same simulation was run, with the convergence threshold modified from the “moderate” setting to “tight.” The number of iterations required for convergence increased slightly (from 335 to 371), however this resulted in very little difference in the deviation between experimental and simulated results. It is assumed that changing this convergence threshold criterion does not have a significant effect on the solution with default settings. However, when the set-up parameters become more advanced and the solution becomes more complex, this setting will have a larger impact in the accuracy and robustness of the solution.

Trial 2 - Manual Mesh Refinement on Balconies

Next, the mesh distribution on the balconies was manually refined with smaller element sizes and a denser distribution. The setting was adjusted to the software’s most refined setting (0.2). All other mesh distributions in the model were left unchanged from the automatic sizing previously applied.

Meshing: Automatic Sizing (“Autosize”) with manual refinement of balconies.

Table 7: Trial 2 finite element summary

	Fluid	Solid	Total
Number of Nodes	71,788	17,870	89,658
Number of Elements	26,362	127,672	391,293

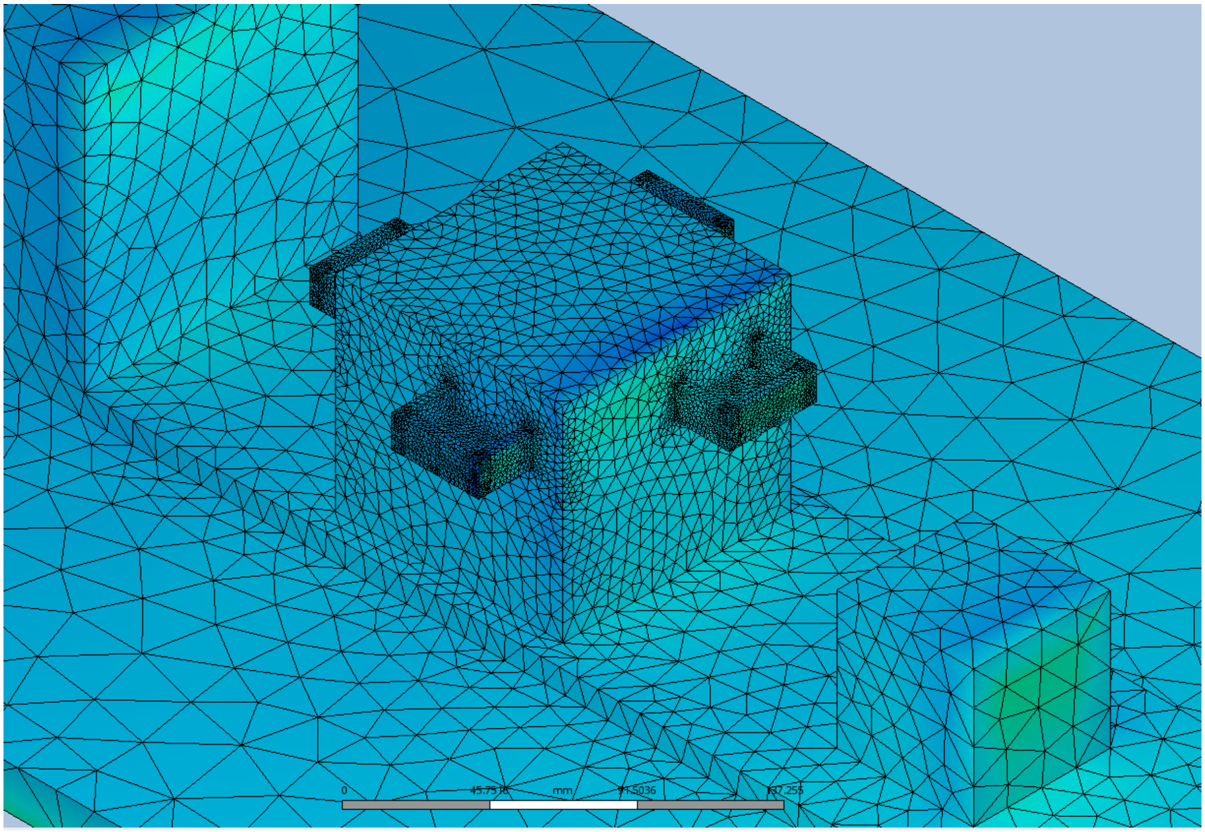

Figure 21: Trial 2, mesh refinement of balconies

Wall Layer Enhancement Settings:

- Wall blending: Off
- Number of Layers: 3
- Layer Factor: 0.45
- Layer Gradation: Auto

Turbulence Model: k-epsilon

Solution Control (Convergence Threshold Criteria): Moderate

Advection Scheme: Monotone streamline upwind (ADV-1)

Number of Iterations for Solution Convergence: 568

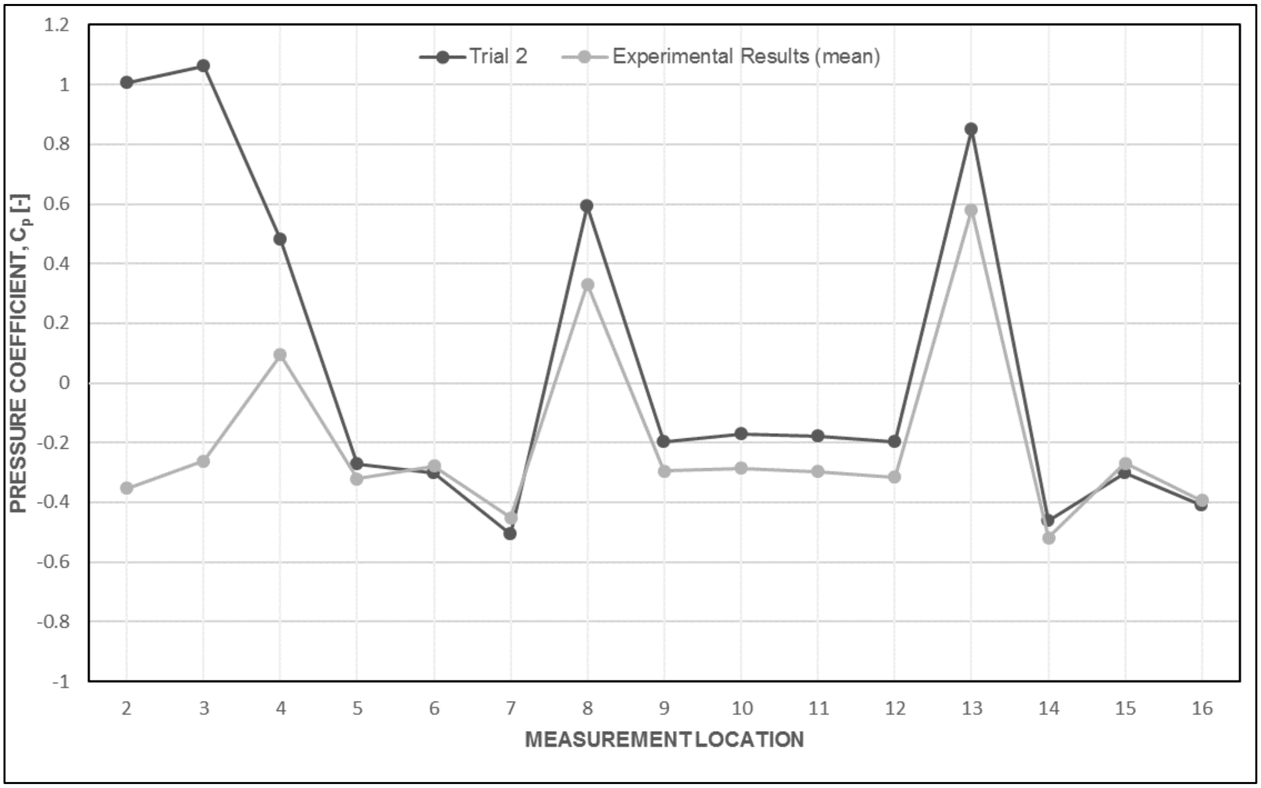

Figure 22: Trial 2 - Manual mesh refinement

As can be seen, Trial 2 resulted in significant improvement in accuracy at measurement points 5, 6, 7, 8, and 16. This is directly a result of refining the mesh at the location of interest (the balconies). Trial 2 resulted in absolute differences of pressure coefficient of less that 0.06 at six measurement locations (5, 6, 7, 14, 15, 16), and as low as 0.014 at measurement location 16.

Note that measurement location 13 decreased in accuracy from the Trial 1 results. This observation is unexplained, but suggests that the accuracy of the result observed in Trial 1 was a coincidence. It was also observed that measurement locations 2 and 3 displayed similar results to Trial 1, suggesting that an inaccuracy is present within the physics of the simulated flow, and not the mesh geometry.

It is predicted that a more accurate solution could be developed by refining the mesh in other regions of relatively complex flow such as the convex corners of the buildings, and wake regions. This is explored in Trial 3.

Trial 3 - Mesh Adaptation

Meshing: Automatic Sizing ("Autosize") with mesh adaptation enabled

Table 8: Trial 3 finite element summary

	Cycle #	Fluid	Solid	Total
Number of Nodes	**1**	16,142	1,986	18128
	2	46,948	4,006	50,954
	3	70,763	5,478	76,241
	4	101,489	9,782	111,271
Number of Elements	**1**	58,862	15,770	74,632
	2	194,636	31,207	225,843
	3	300,135	42,524	342,659
	4	439,279	71,680	510,959

Mesh Adaptation Settings:

- Number of cycles: 3
- Allow Coarsening: On
- Flow Angularity: On
- Free Shear Layers: On
- External Flow: On
- Transient Features: Off

Wall Layer Enhancement Settings:

- Wall blending: Off
- Number of Layers: 3
- Layer Factor: 0.45
- Layer Gradation: Auto

Turbulence Model: k-epsilon

Solution Control (Convergence Threshold Criteria): Moderate

Advection Scheme: Monotone streamline upwind (ADV-1)

Number of Iterations for Solution Convergence:

Cycle #1 (base case): 333

Cycle #2: 428

Cycle #3: 506

Cycle #4: 678

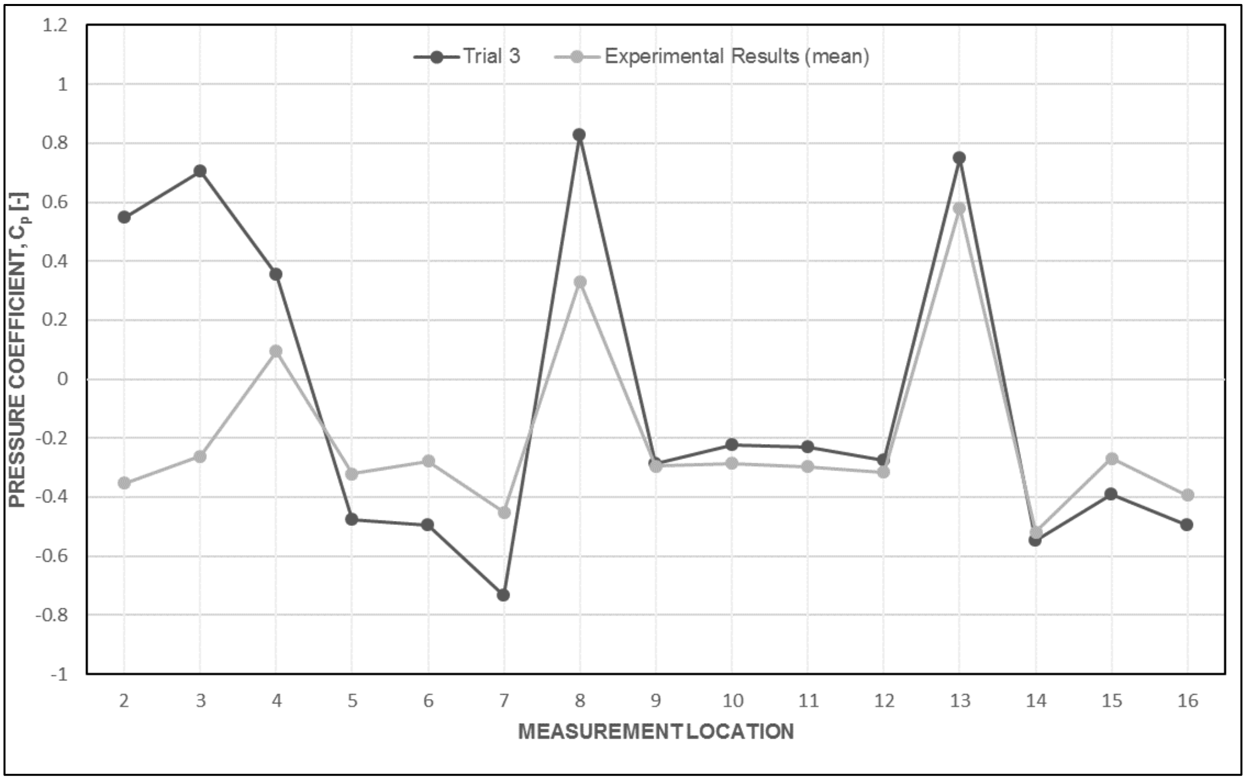

Figure 23: Trial 3 - Mesh adaptation

Enabling mesh adaptation (3 cycles) produced a mesh distribution that is refined in several regions to varying degrees. As can be seen in Figure 24, which depicts the final mesh produced for the third cycle, the mesh has been automatically refined in regions of complex flow such as convex corners and wake regions throughout the model. Note that as the mesh becomes more complex, more iterations are required for convergence of the solution as expected.

Mesh adaptation produced an interesting result with varying degrees of accuracy improvement when compared to manual mesh refinement (Trial 2). Like in Trial 2, improvements in accuracy from Trial 1 could be observed at measurement locations 5, 7 and 16, however not to the same degree as in Trial 2. The improvements seen in Trial 2 at locations 6 and 8 were not observed in this trial. Trial 3 did however produce improvements in locations 9, 10, 11 and 12, where absolute differences in pressure coefficient were less than 0.07 and as low as 0.01 (location 9), whereas Trial 2 did not.

The results of this trial suggest that the mesh adaptation feature in this software does not necessarily produce the mesh that is desired and that will produce the most accurate results. In this case, slightly more overall accuracy is obtained by manually refining the mesh.

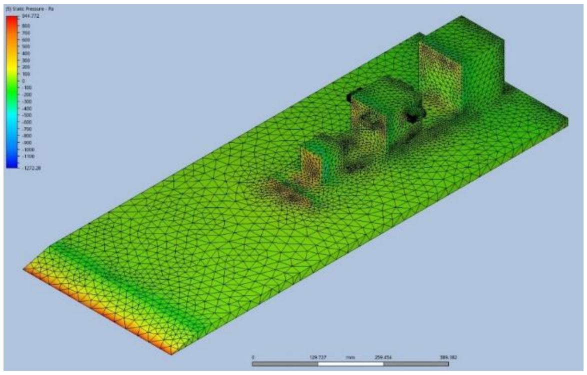

A

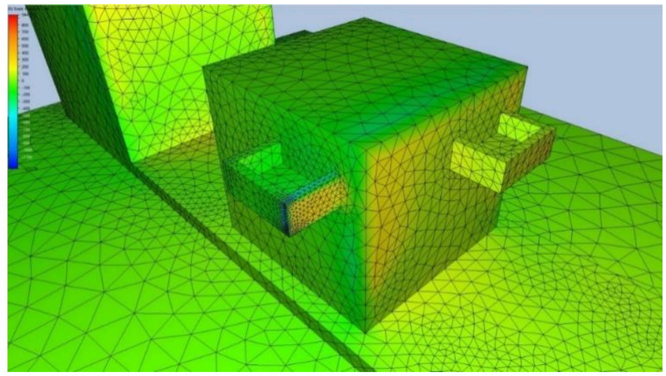

B

Figure 24: Mesh adaptation, final cycle

Trial 4 - Modified Turbulence Model (SST k-omega)

As mentioned in Section 5.2, the SST k-omega turbulence model does not use wall functions, but instead simulates turbulence in all regions approaching a wall. Therefore, in order to produce an accurate solution, the mesh needs to be manually modified in the boundary layer at all fluid-wall and fluid-solid interfaces. This is done by blending the transition between the wall layers and the adjacent mesh, adding additional layers, controlling the layer thickness ("layer factor") and layer growth rate ("layer gradation"). Note the increase in number of mesh nodes and elements (Table 9) in comparison to the automatic mesh generated in Trial 1. Also note that it is recommended that the Modified Petrov-Galerkin advection scheme (ADV-5) be used with the SST k-omega turbulence model and is also recommended for external flow.

Meshing: Automatic Sizing ("Autosize")

Table 9: Trial 4 finite element summary

	Fluid	Solid	Total
Number of Nodes	57,611	8,934	66,545
Number of Elements	235,910	51,424	287,334

Layer Enhancement Settings:

- Wall blending: On
- Number of Layers: 10
- Layer Factor: 0.60
- Layer Gradation: 1.25

Turbulence Model: SST k-omega

Solution Control (Convergence Threshold Criteria): Moderate

Advection Scheme: Modified Petrov-Galerkin (ADV-5)

Number of Iterations for Solution Convergence: 547

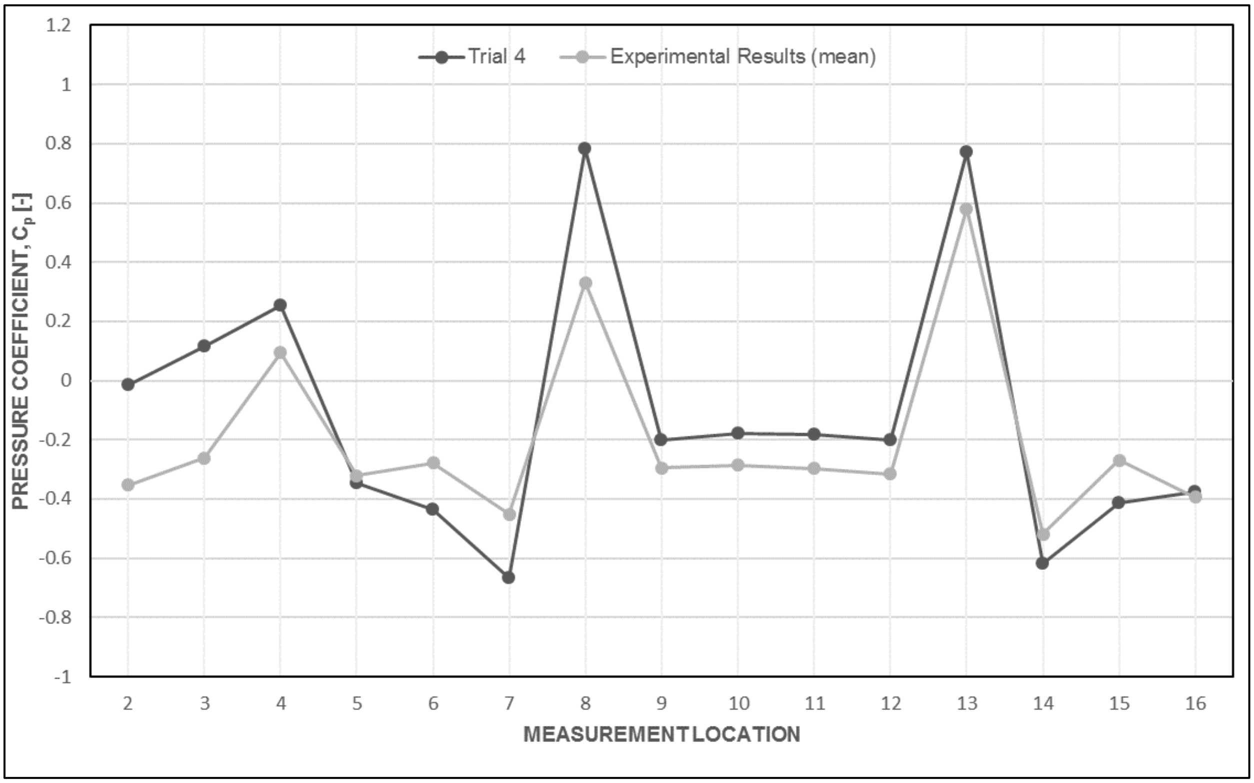

Figure 25: Trial 4 - Modified turbulence model

The most notable improvement in accuracy with Trial 4 can be seen at measurement points 2 and 3. With the change of turbulence model from k-epsilon to SST k-omega, the mean pressure coefficients of these two points has decreased significantly from Trial 1. It can be seen that the experimental and simulated results of these two points now follows a similar trend. The relative difference between experimental and simulated results for location 2 and 3 is still quite large, however, this deviation is expected to decrease further when combined with the appropriate mesh refinement settings. From these results the conclusion can be made that the physics of the flow were not being simulated properly using the software's default turbulence model. This produced an unrealistic wake region, generated by the small building, that resulted in mean positive pressure measurements at locations 2 and 3, when in reality this wake produced mostly negative pressures at this location. Trial 4 demonstrates that the selection of an appropriate turbulence model is critical in producing an accurate solution in Autodesk CFD, and cannot be overlooked.

Improvements in accuracy from Trial 1 can also be seen at measurement locations 4, 5, 6, 7 and 16, especially location 5 which achieves an absolute difference in pressure coefficient of 0.018, the lowest of all the trials for that location.

Final Simulation Model

After performing the above analysis on the Autodesk CFD parameters, an ideal combination of these settings was developed which most accurately represented the flow condition in the experimental wind tunnel. The results from this analysis are very useful and can be used to produce an accurate solution in a similar external flow scenario, on a larger and more complex scale.

The simulation that produced the most accurate solution used the SST k-omega turbulence model with a manually refined mesh on the balconies and the regions upwind from the middle building. The mesh refinement was intended to combine the improvements of accuracy seen from the manual balcony mesh refinement, and the refinement of surrounding regions seen when utilizing mesh adaptation. Note that the highest number of nodes and elements are used in the meshing of the final simulation model.

Meshing: Automatic Sizing ("Autosize") with manual mesh refinement of balconies.

Table 10: Final simulation finite element summary

	Fluid	Solid	Total
Number of Nodes	176,423	42,629	219,052
Number of Elements	743,216	256,994	1,000,210

Layer Enhancement Settings:

- Wall blending: On
- Number of Layers: 10
- Layer Factor: 0.65
- Layer Gradation: 1.25

Turbulence Model: SST k-omega

Solution Control (Convergence Threshold Criteria): Tight

Advection Scheme: Modified Petrov-Galerkin (ADV-5)

Number of Iterations for Solution Convergence: 1,846

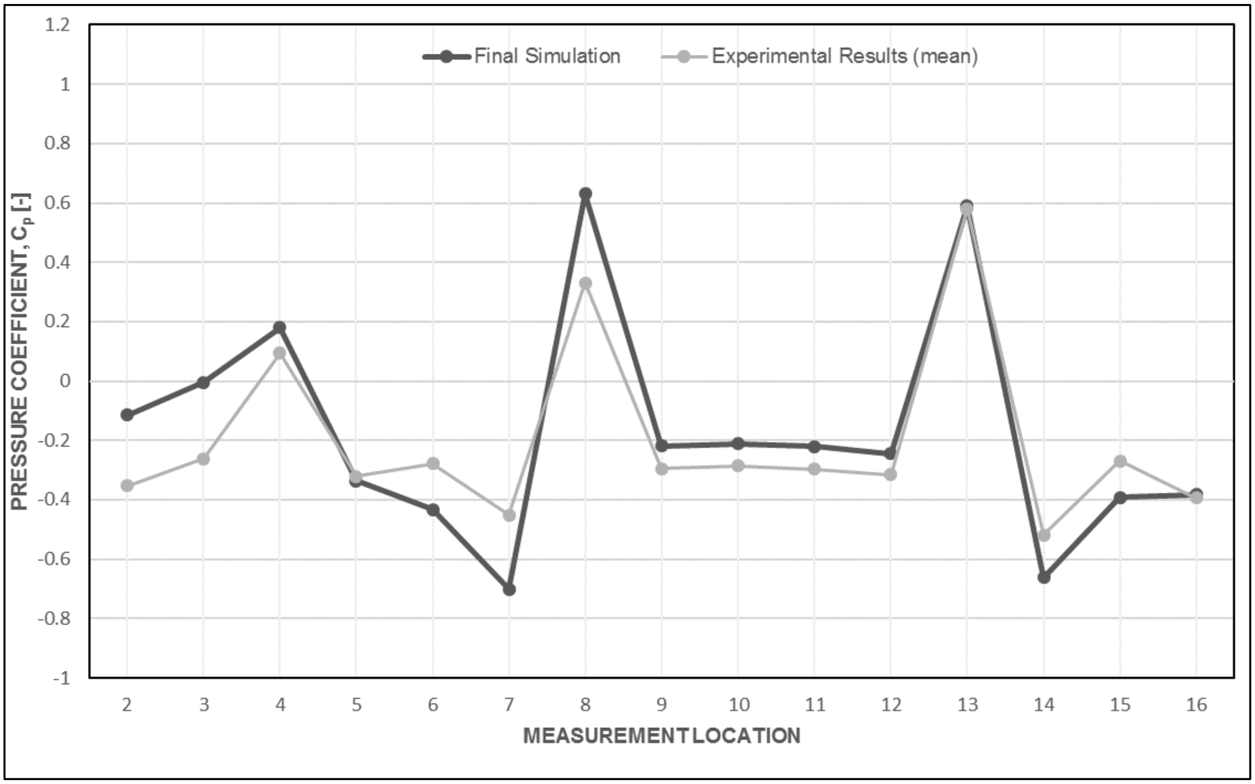

Figure 26: Trial 5 - Final simulation

In the final simulation, measurement locations 2 and 3 display a negative mean pressure coefficient for the first time in the sensitivity analysis. Other measurement locations (4, 5 ,13 and 16) achieved the highest accuracy and lowest absolute difference in pressure coefficient when compared to the results of the other trials. Although accuracy was lost at some measurement locations, for example at 6 and 7, the overall accuracy of the solution is high. The average difference in pressure coefficient between experimental and simulated results for all measurement locations is 0.125, which is relatively high. The high value is a result of differences seen at locations 2, 3, 7 and 8 that display absolute differences in pressure coefficients of greater than 0.2. Nevertheless, the general common trends between experimental and simulated results can clearly be seen.

Several important conclusions were made from the sensitivity analysis. First of all, it was noted that the modification of the convergence criteria from a “moderate” to “tight” setting has a significant impact on the accuracy of the solution in an advanced and customized set-up such as this. The number of iterations required for convergence increased to 1,846.

A major conclusion from this analysis was that the refinement and modification of the mesh in complex flow regions and regions of interest is critical in producing an accurate solution. This can be done by manually refining the mesh, by using the mesh adaptation feature, or by using a combination of both. The other significant conclusion made in this analysis was that the selection of turbulence model being used in the simulation is critical to a meaningful and accurate representation of flow. The use of the SST k-omega turbulence model and its associated settings (ADV-5 and wall layer enhancement) provided the most accurate solution for this flow type and for external flow applications.

5.2.3 Summary

Using Autodesk CFD's default settings, especially settings related to meshing and turbulence modelling, often produces inaccurate results, depending on the simulation type. For this software, and all simulation software in general, it is highly recommended that a thorough understanding of the software, it's set-up and settings be achieved before proceeding with any simulation or data collection.

As discussed, the average difference in pressure coefficient between experimental and simulated results for all measurement locations is 0.125. Maximum absolute difference in the final simulation occurs at measurement location 3 (0.257) and minimum absolute difference occurs at measurement location 13 (0.007). However, location 3 also displays the highest degree of relative improvement over the five simulation trials, as can be seen in Table 11. Note again that each trial does not represent the accumulative change in multiple settings, but represents the changing of a single CFD parameter or setting. Therefore, it is expected that an overall decrease in absolute difference will not be seen from trial to trial. The final simulation is the cumulative result of the change of all mentioned parameters.

Table 11: Sample difference between experimental and simulated results over all trials

Trial	Measurement Location 3 (ΔC_p)	Measurement Location 13 (ΔC_p)
1	1.21	0.097
2	1.32	0.270
3	0.964	0.168
4	0.374	0.202
Final	0.257	0.007

Sources of Error

Seeing as the average difference in pressure coefficient between experimental and simulated results of all measurement locations is 0.125, sources of error must be discussed. Although certain measures were taken in an attempt to limit experimental error, some significant potential sources of error could not be addressed. The majority of these sources of error are a direct result of scaling issues. The scale of the model was limited due to the size of the available wind tunnel, and many of the errors discussed below would be mitigated or eliminated with the use of a larger wind tunnel and model.

Losses in pressure within the balcony models and wind tunnel model were not accounted for. All materials used to construct the wind tunnel model had some degree of porosity, which allow slight amounts of air flow through them, producing a decrease in measured surface pressure. The CFD software used does not take this into account. The 3D printed balconies, where measurements were taken, consist of ABS plastic which has been printed in layers in a dense hatching pattern. The finished product, although dense, is in fact slightly porous due to this manufacturing process. The porosity of these components should be accounted for in calculations or by coating the components in an air impermeable layer, such as latex paint. Due to the small, detailed geometry of the balconies used in the model, this was not possible.

The balcony holes leading to the tubulation connection contained two elbow joints (90° turn) each. Geometries such as this are not ideal for pressure measurement situations, as the connection presents a scenario where the flow is altered and can be reflected upon itself. This was accounted for in the design of the joints by reducing the angle as much as possible, smoothing the transition between axial planes. If the geometry was larger in scale, the transitions would be even smoother and this effect would be reduced further.

Holes and cavities in 3D printed components, such as holes within the balconies, are filled with a support material during the printing process to ensure stability of the cavity while printing is completed. The 3D printed component is then immersed in a chemical solution designed to dissolve only the support material. Although attempts were made to clear the holes of any remaining support material, ensuring the complete removal of this material was not possible due to the small scale of the component. Any blockage of the balcony holes would have caused an inaccuracy in the experimental pressure measurements.

Due to the layout and geometric limitations to the wind tunnel, long sections of pneumatic tubing were required to make the connection between the edge of the balconies to the pressure transducer. Long sections of tubing presents multiple potential issues. First of all, as the length of the connection increases, the likelihood of a disruption or defect in that connection increases. The use of relatively long lengths of tubing leads to a modification of the pressure at the transducer compared to that at the model surface [17].

Finally, in order to obtain a more accurate representation of the average pressure profile on each balcony surface, more pressure taps would be installed per balcony. The experiment was limited to 15 pressure measurement taps. More pressure taps would require detailed consideration of additional equipment and connection logistics, in addition to a model that is larger in scale.

6. CFD Analysis of the Shangri-La Hotel

The next sections describe the various set-up parameters and settings used in the CFD simulation of the Shangri-La Hotel.

6.1 Historical Wind Data Analysis

When performing an investigative study, historical wind data from the time of building completion to the time of failure can be used to analyze the known locations of failure on the building. However, if this methodology was to be used as a tool to identify problematic locations on a façade in order to prevent future occurrences, wind speeds and directions which represent the average and most common local conditions must be considered. In addition to these average conditions, the extreme conditions of high wind speed should also be analyzed.

For the purposes of this paper and case study, a historical wind data analysis was performed for a two-year period from the date of building completion (July 2012) to the date of each balcony guard failure (up to July 2014). Hourly wind data was extracted from the Environment Canada database, using Toronto's Billy Bishop Airport (YTZ) as the location. The YTZ weather station was selected due to its proximity to the Shangri-La Hotel (< 3 km), and because it is an airport which means a wide range of accurate and reliable data is available. The weather station is at an elevation of 76.8m above sea level, which results in an atmospheric pressure of 100.4 kPa, at 15°C.

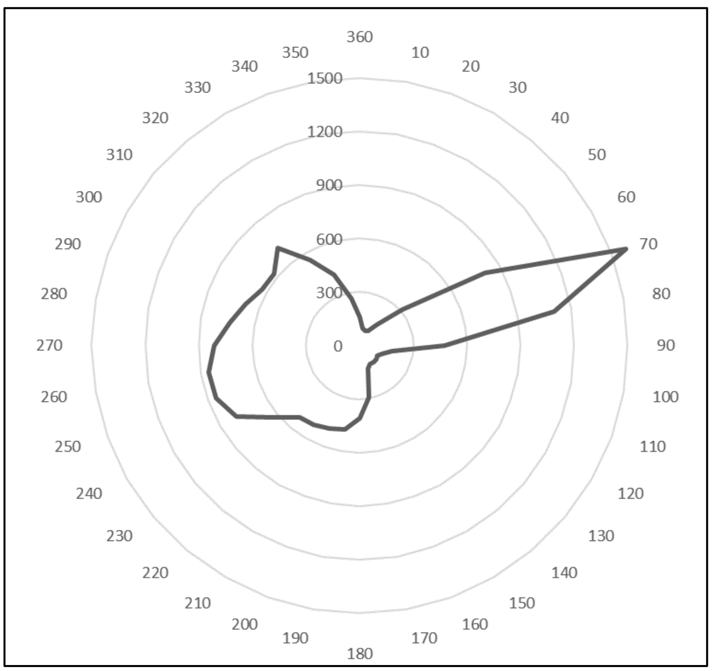

Figure 27: Wind rose (YTZ airport), July 2012 to July 2014 (radial units: hours)

The most common wind direction experienced is consistently from the Northeast (70° from North), and second most common wind directions are from the Southwest (250° to 270° from North). Note, all wind directions in this report are specified in clockwise degrees from North.

Several significant periods of gust conditions were observed from July 2012 to July 2014. For example, in January 2014 wind speeds of above 20 km/h, and up to 72 km/h, were maintained for a period of almost seven days, resulting in a weekly average wind speed of 39 km/h. These high wind speeds were consistently from the Southwest (210° to 290°). Another month of high average wind speeds was April 2013, which had a recorded maximum gust condition of 89 km/h from the Northeast (70°).

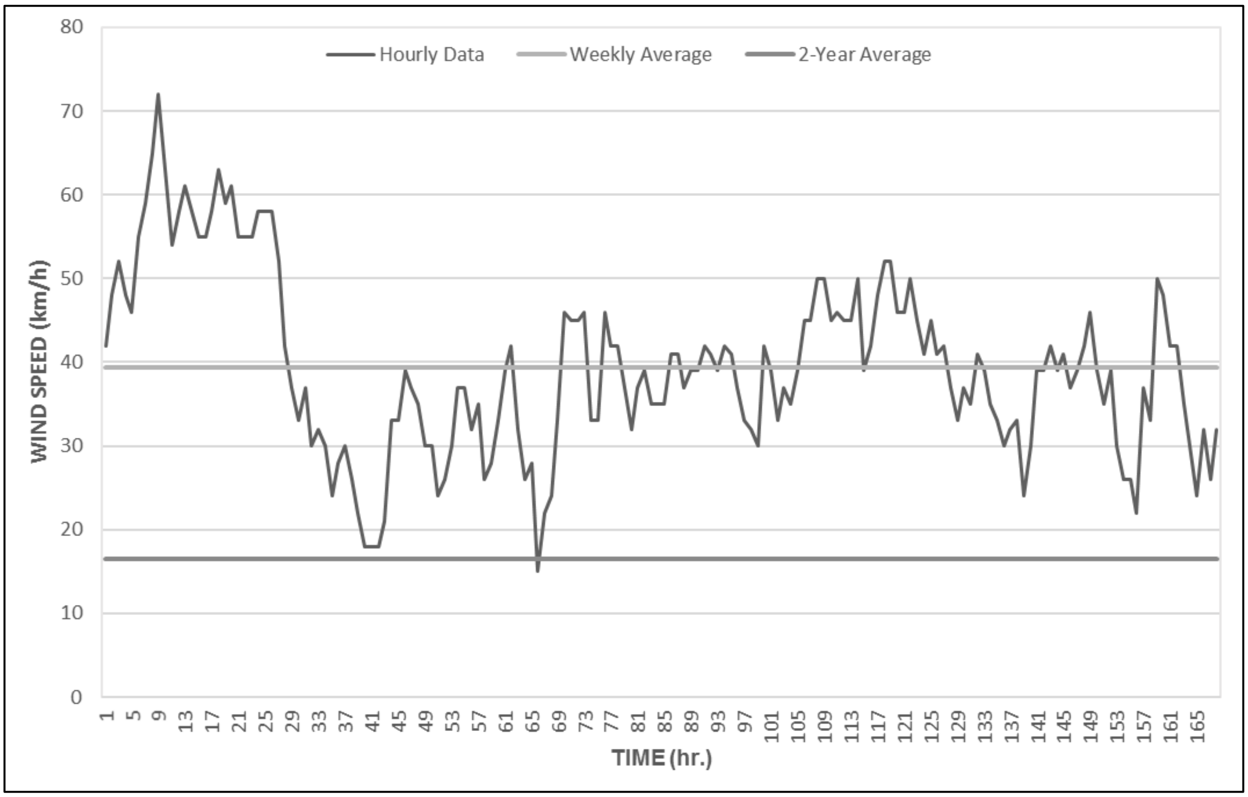

Figure 28: Gust condition, January 24th to 31st, 2014

It can be seen that the average wind speed for each date range remains relatively consistent and is between 16 and 17 km/h. Variations in air density, due to seasonal temperature changes must also be taken into account. For this reason, average temperatures were calculated for each time period, and temperatures were recorded for the gust conditions.

Table 12: Historical wind analysis summary

	Failure Location #1	Failure Location #2	Failure Location #3	Failure Location #4
Date of failure	Jan. 23, 2013	Sept. 10, 2013	Nov. 24, 2013	July 17, 2014
Floor/Facade	37/South	23/East	23/South	51/East
Date Range	July 2012 – Jan. 2013	July 2012 – Sept. 2013	July 2012 – Nov. 2013	July 2012 – July 2014
Avg. wind speed, km/h (m/s)	16.1 (4.5)	16.1 (4.5)	16.4 (4.6)	17.1 (4.8)
Common Wind Directions	70°, 270°, 250°	70°, 270°, 320°	70°, 270°, 250°	70°, 260°, 250°
Avg. temp. (°C)	11.1	11.4	10.9	8.8
Gust Condition	48 km/h at 250°	89 km/h at 70°	N/A	72 km/h at 220° and 240°

After this analysis, it was determined that the following six scenarios would be considered in order to accurately represent the wind conditions for the period of interest. It can also be assumed that based on this two-year study, these scenarios accurately represent the average wind conditions experienced in the downtown Toronto area.

Table 13: CFD simulation scenarios

Wind Direction	Average Wind Condition, km/h (m/s)	Extreme/Gust Condition, km/h (m/s)
70°	16.9 (4.7)	89 (24.7)
220°	16.9 (4.7)	72 (20)
250°	16.9 (4.7)	72 (20)

6.2 Set-Up: Autodesk CFD

In order to create the full scale 3D model that would be imported into the CFD software, 3D massing files provided as open source data by the City of Toronto Planning department were used as a basis. The block of interest, that contained the Shangri-La Hotel and the surrounding buildings (‘50G_N_2’), was downloaded as a Sketchup file. This 3D model contained buildings and details which were unnecessary for the purposes of this simulation, and result in vast computational processing power. The surrounding buildings were simplified to basic masses which represented the overall building footprint (Figure 29).

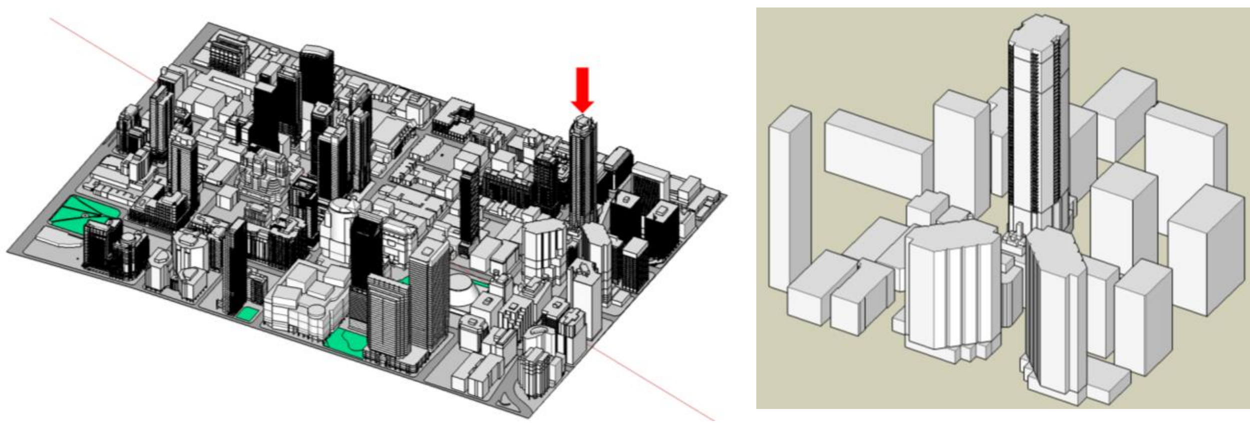

A *B*

Figure 29: Simplification of 3D massing geometry, original (A), simplification (B)

A more detailed, but similar approach was used for the Shangri-La Hotel itself. The Shangri-La Hotel was vertically divided into five slightly different sections, which represented how the building plan changes with height. Unnecessary geometry features, such as the rooftop mechanical and HVAC spaces, were removed (Figure 30). The Shangri-La Hotel balcony geometry provided by the City of Toronto was left unchanged, except the balcony guards of interest were divided into sections to represent each pane of glass.

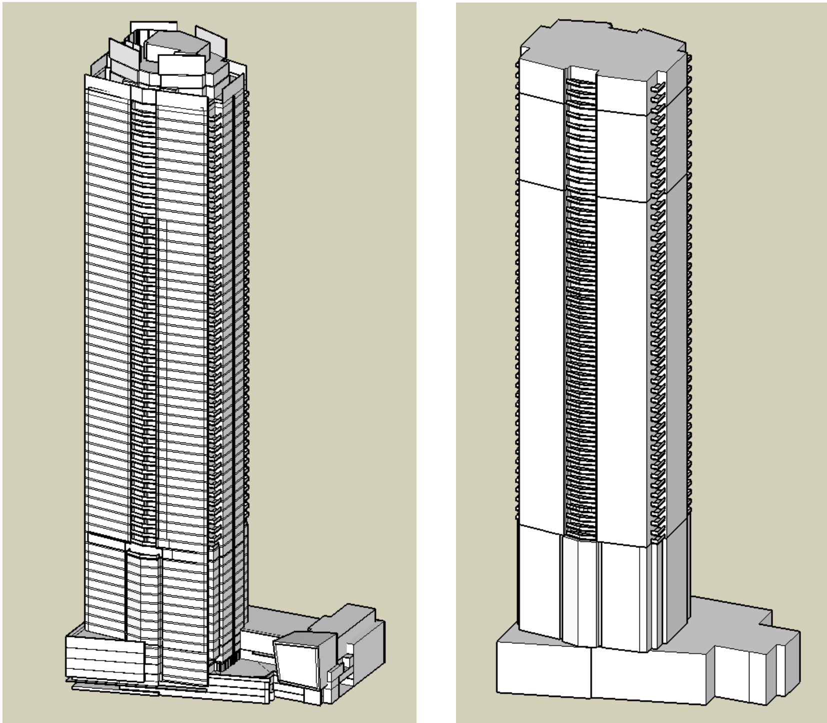

A B

Figure 30: Simplification of the of Shangri-La Hotel 3D massing geometry, original (A), simplification (B)

To simulate external flow in CFD software, an external volume, which represents the air volume, must be created and must fully surround the model. This external volume was created as part of the 3D model in Sketchup, as opposed to in the CFD software. When the external volume was created in CFD software, it was impossible make it co-planar with the “street level” or bottom surfaces of the buildings. This is important because it provides correct simulation of the ground plane and does not allow unrealistic air flow underneath buildings. The dimensions of the external air volume were created based on recommended proportions by Autodesk [27] for external flow (Figure 31), which resulted in a volume with dimensions 1,725 m x 2,150 m x 600 m. The external volume was rotated in order to simulate wind conditions from various angles of attack.

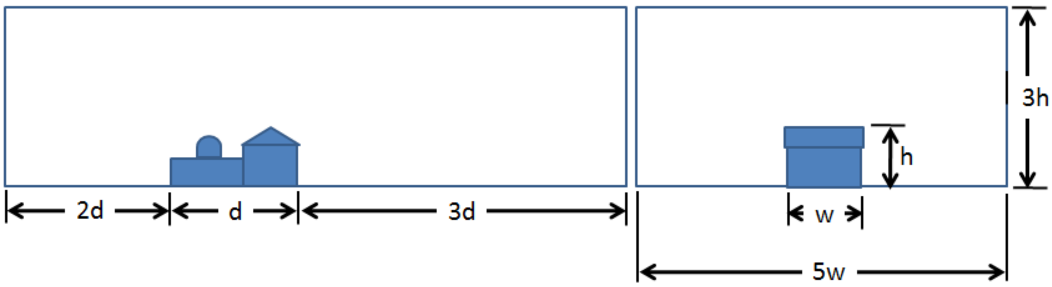

Figure 31: Recommended dimensions of external volume

Once the model was successfully imported into Autodesk CFD, set-up parameters were applied which reflected the wind tunnel validation study performed in Section 5. First, to further simplify the model and help prevent meshing errors, edges less than 10° were merged and small objects were removed using the program's built in "Geometry Tools".

Next, materials were assigned to all volumes. Since only simplified masses and geometries were used to create the model, it was only possible to assign one material to each volume, which was chosen to be glass. Glass is the most common exterior envelope material that the wind interacts with in these type of buildings, justifying the generalization. The external volume was assigned as an air volume, with environment conditions, such as temperature and pressure, that could be changed based on the scenario.

The external air volume was then assigned various boundary conditions to simulate wind moving through the space. As in the validation study, the top surface and sides were set to a "slip/symmetry" boundary condition, and the outlet surface was assigned a zero gage pressure (static) condition. The bottom surface (ground plane) was not assigned a boundary condition, which means the software will assume a "wall" condition, meaning flow cannot pass through the plane.

For the inlet velocity condition, a height dependent profile was created in order to simulate a realistic flow that has been altered by the surrounding environment and terrain roughness. The airport station used in this analysis is in downtown Toronto and adjacent to Lake Ontario. This must be accounted for when representing the wind and flow condition measured at the weather station and the flow approaching the Shangri-La Hotel, which is surrounded by tall buildings. The relationship between wind speed, V_z, and height, Z, due to various terrain categories, can be represented by a power law, with appropriate exponents [33].

$$\frac{V_z}{V_g} = \left[\frac{Z}{Z_g}\right]^{\alpha} \tag{15}$$

$V_z = mean\ wind\ speed\ at\ any\ height$

$V_g = freestream\ velocity\ at\ the\ edge\ of\ a\ boundary\ layer$

$Z_g = boundary\ layer\ thickness$

$\alpha = mean\ wind\ speed\ exponent$

The mean wind speed exponent (α) varies from values as low as 0.1 for smooth terrain such as a lake, to 0.4 for city centers. The velocity profile for a gust condition is represented by the same power law, however different exponents (β) are used, which creates a different velocity profile. Examples of these various exponents are shown below in Table 14 [33].

Table 14: Values of gradient height and power law exponents for wind profiles [33]

Terrain category and description	Gradient height (Z_g)	Mean speed exponent (α)	Gust speed exponent (β)
1. Open sea, ice, tundra, desert	250 m	0.11	0.07
2. Open country with low scrub or scattered trees	300 m	0.15	0.09
3. Suburban areas, small towns, well wooded areas	400 m	0.25	0.14
4. Numerous tall buildings, city centers, well-developed industrial areas	500 m	0.36	0.20

For the purposes of this simulation values from Category 4 (numerous tall buildings, city centers, well developed industrial areas) were assumed for the Shangri-La Hotel's location (α = 0.36 and β = 0.20). However, for the airport weather station location values from Category 3 were used (α = 0.25 and β = 0.14). This assumption was made because of the airport's various surroundings: Lake Ontario (Category 1) to the South and East and downtown Toronto (Category 4) in all other directions. It was also assumed that wind velocity measurements were taken from a weather station at 10m in elevation. Using the mean wind condition of 17 km/h (4.7 m/s) as an example, the various velocity profiles were calculated as follows:

At the wind speed measurement location (YTZ airport), the freestream velocity at the edge of the boundary layer was calculated. Note that in this location (Category 3) the boundary layer is 400 m high.

$$\frac{V_z}{V_g} = \left[\frac{Z}{Z_g}\right]^{\alpha} \rightarrow V_g = \frac{V_z}{\left[Z/Z_g\right]^{\alpha}} = \frac{4.7\ m/s}{[10\ m/400\ m]^{0.25}} = 11.8\ m/s$$

This freestream velocity could then be applied to the Shangri-La Hotel's location in order to calculate the velocity profile in the downtown core. Note that the freestream velocity, V_g in this situation occurs at the edge of the boundary layer which is now at 500 m it height. The velocity at any height, Z, was then calculated using the relationship:

$$V_z = V_g * \left[\frac{Z}{Z_g}\right]^{\alpha} = 11.8\ m/s * \left[\frac{Z}{500\ m}\right]^{0.36}$$

The three different velocity profiles (average and gust conditions) used as inlet boundary conditions for CFD simulations are shown in Figure 32.

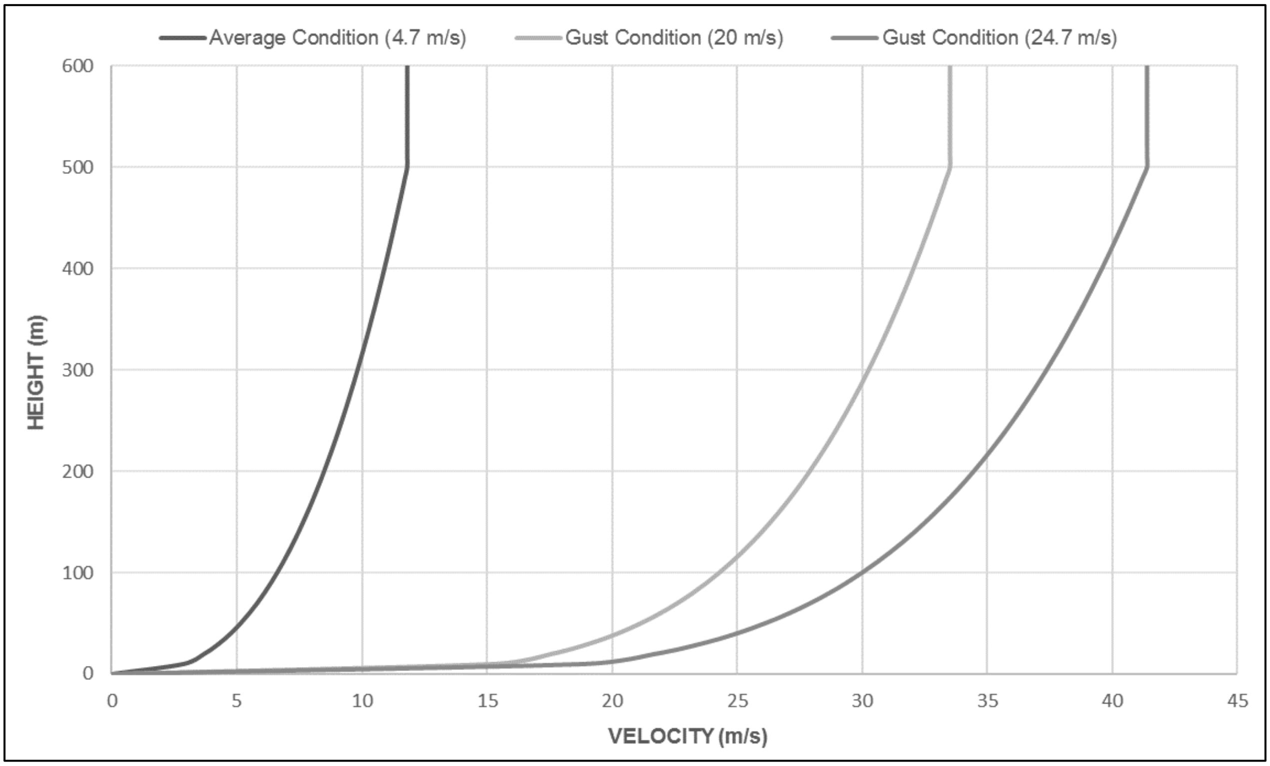

Figure 32: Velocity profiles, CFD inlet boundary condition

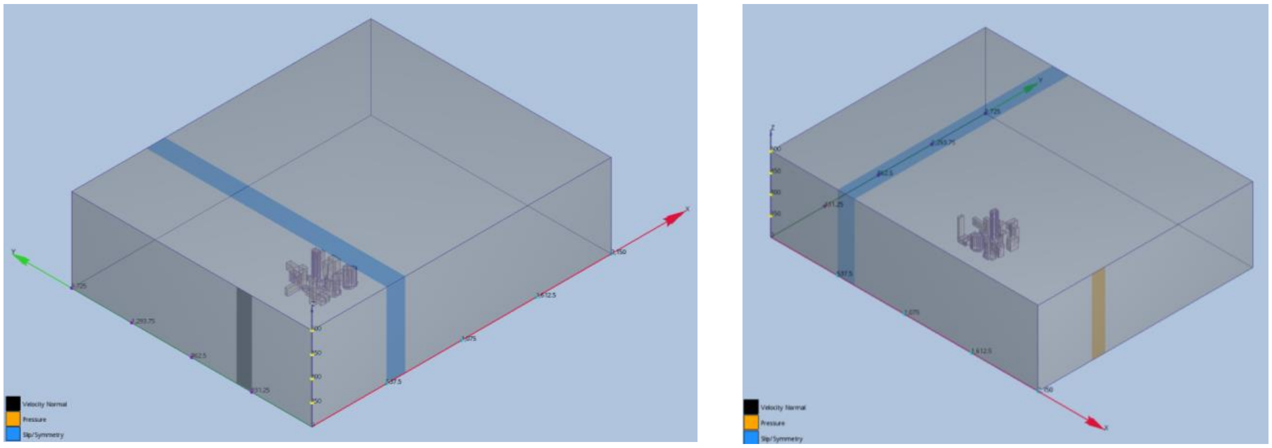

A *B*

Figure 33: CFD model with boundary conditions

Additional set-up and modification of settings and parameters were applied based on the results of the CFD validation study, and are discussed in Section 6.2.

The pressure coefficient was calculated at each balcony guard failure location using the following equation:

$$C_p = \frac{P}{0.5\rho U^2} \tag{16}$$

$P = average\ static\ surface\ pressure\ [Pa]$

$\rho = air\ density\ [kg/m^3]$

$U = freestream\ velocity\ [m/s]$

The average surface pressure at each location was determined using the software's "wall calculator" function. Where exact failure location was not known, an average was taken for all of the balcony guard panes. Air density was determined based on the ambient condition (air temperature) of each scenario. Freestream velocity had to be calculated from the velocity profiles for each failure location and is displayed below in Table 15.

Table 15: Wind speed at failure location height

Floor # (height)	Average Condition (4.7 m/s)	Gust Condition (20 m/s)	Gust Condition (24.7 m/s)
23 (60 m)	5.5 m/s	21.9 m/s	27.1 m/s
37 (102 m)	6.6 m/s	24.3 m/s	30 m/s
51 (144 m)	7.5 m/s	26 m/s	32.1 m/s

6.3 Results and Discussion

The following set-up parameters and simulation settings were used for all CFD simulations presented in this section. The selection of these settings was based on the results of the CFD validation study performed in Section 5.

Turbulence Model: SST k-omega

Advection Scheme: Modified Petrov-Galerkin (ADV-5)

Solution Control (Convergence Threshold Criteria): Tight

Meshing:

From the validation study it was concluded that refinement of the mesh in certain areas of interest increased the accuracy of the solution drastically. Therefore, the mesh was refined on every balcony on the model, which resulted in a meshing pattern as shown below in Figure 34. The other volumes in the model were assigned an automatically sized mesh determined by the software.

Table 16: Finite element summary

	Fluid	Solid	Total
Number of Nodes	466,136	52,180	518,316
Number of Elements	1,217,363	382,624	1,599,987

Wall Layer Enhancement Settings:

As previously mentioned in Section 5.2, when using the SST k-omega turbulence model, modifications must be made to the mesh generated in the boundary layer in order to generate an accurate solution. The mesh was enhanced as before by increasing the number of layers to 10, the layer factor to 0.45 and the layer gradation was changed from “Auto” to 1.25. When boundary layer blending was enabled, it produced an error when generating the mesh. It is assumed that this feature is too complex at such a large scale.

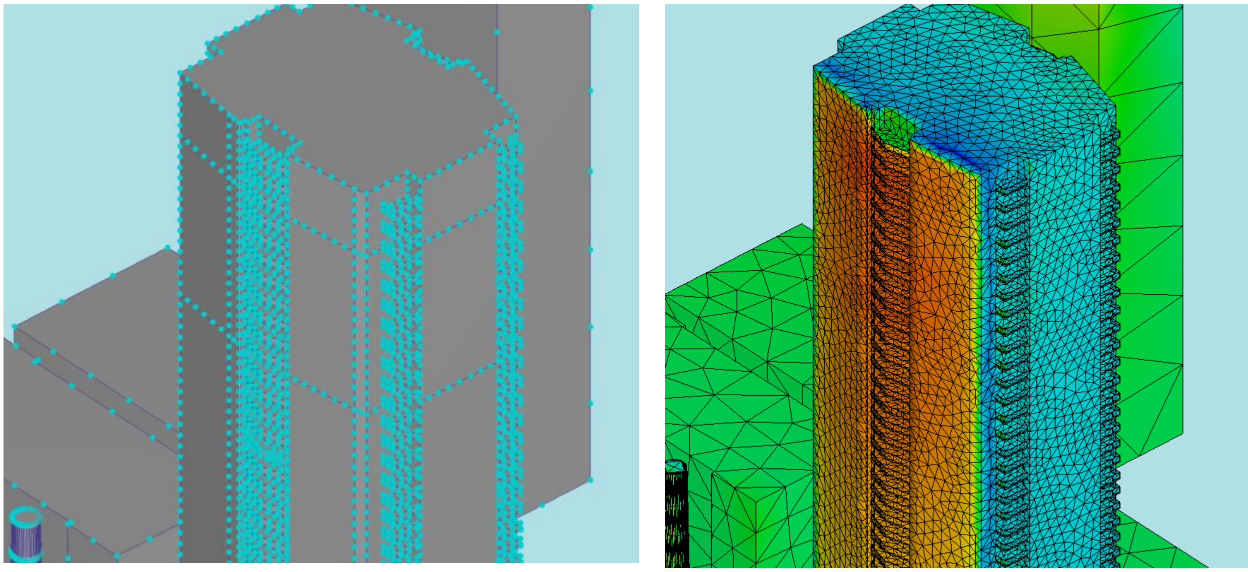

A B

Figure 34: Balcony mesh refinement, nodes (A), pressure results with mesh (B)

A number of initial observations can be made from the simulation results. The most important observation is the correlation between Toronto's overwhelmingly most common wind direction (70°) as found in Section 6.1, and two of the building's balcony guard failure locations on the East façade of the building. Due to Toronto's street axis rotation of approximately 17° from North, the 70° wind direction impacts the East façade of the Shangri-La Hotel directly and perpendicularly. The direct impact results in relatively high surface pressures on the East façade. As wind speed increases with height, as do the surface pressures on the façade, as can be seen in Figure 35. Although the other tested common wind directions (220° and 250°) do not result in the same direct impact on the South façade failure locations, there are still several important observations that will be discussed.

The most common wind directions differ by approximately 180°. The alternating wind directions of 70° and 220°/250° results in alternating positive and negative pressures on the building's East façade. Alternating positive and negative pressures on the balcony guard surfaces is an important factor in the fatigue loading of the glass. The alternating conditions produce a varying and dynamic loading condition that promotes the propagation of embedded cracks in tempered glass.

It can also be initially observed that for some simulation conditions, the lower surrounding buildings block the lower levels of the Shangri-La Hotel from direct impact by the flow. As height is increased, flow becomes uninterrupted and uninfluenced by the surrounding buildings towards the upper floors of the Shangri-La Hotel.

Wind Direction Scenario #1: 70º

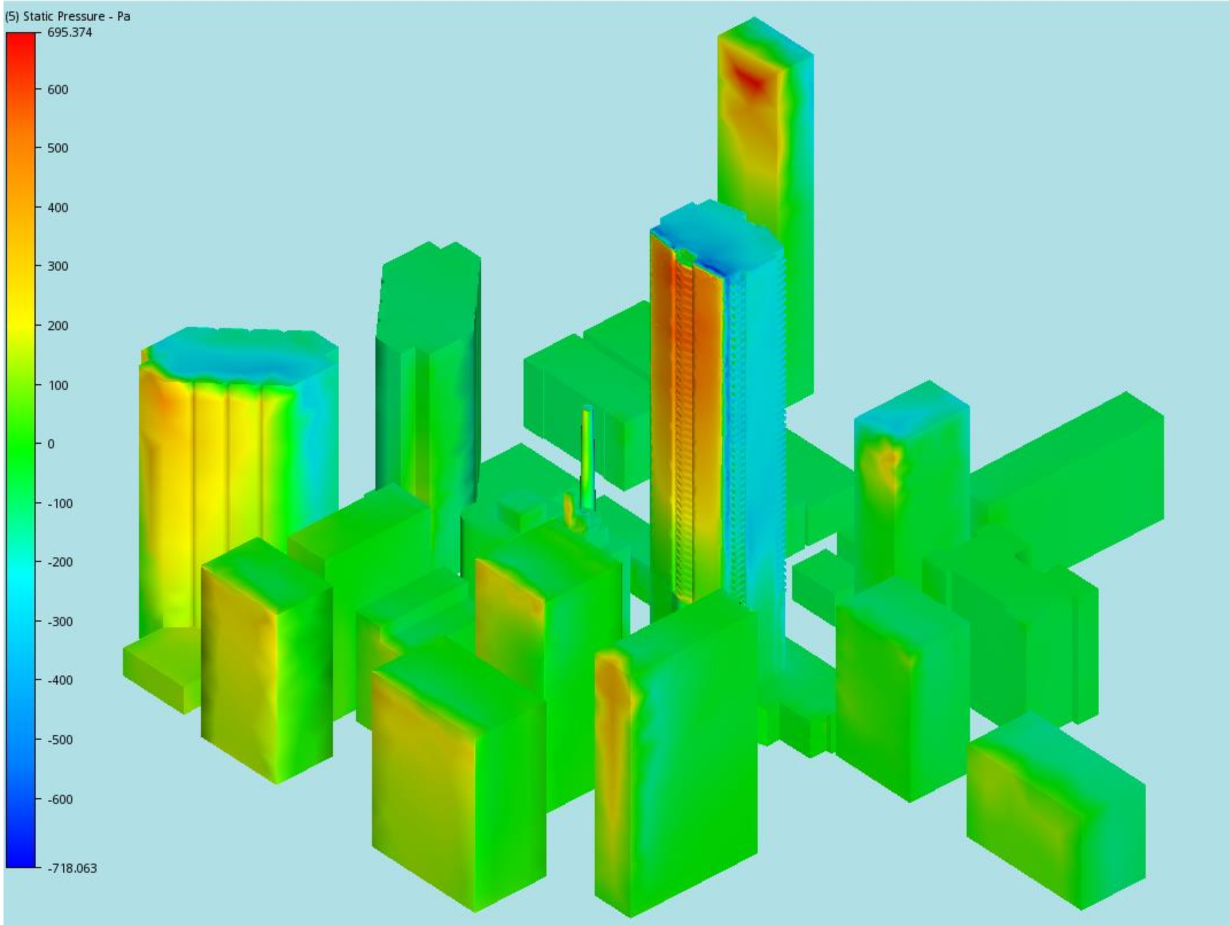

Figure 35: 70°, gust condition

Table 17: 70° CFD results

		Location 1	Location 2	Location 3	Location 4
Floor/Facade		37/South	23/East	23/South	51/East
Average Condition	Surface Pressure [Pa]	-13.9	-0.7	-10.7	21.6
	Pressure Coefficient [-]	-0.64	-0.04	-0.57	0.63
Gust Condition (24.7 m/s)	Surface Pressure [Pa]	-247.2	54.1	-154.3	507.2
	Pressure Coefficient [-]	-0.48	0.12	-0.33	0.78

Number of Iterations for Solution Convergence: 765 (average), 610 (gust)

For the gust condition of 24.7 m/s, wind from a direction of 70° results in surface pressures at failure location 4 (Floor 51/East) of 507.2 Pa (Figure 36), and a pressure coefficient of 0.78. 507.2 Pa is a significant wind induced surface pressure and represents a condition of concern that should be considered and evaluated. Continued exposure to surface pressures in excess of 500 Pa represents a cyclic loading condition that could lead to the weakening of a material. In the case of tempered glass, if a crack is present within the specimen due to an impurity, installation or manufacturing errors, or external factors, a cyclic loading condition of 500 Pa could lead to the eventual propagation of the crack and a potential failure. However, it is clear that under these instantaneous conditions, the theoretical failure strength of tempered glass, which is in the range of mega pascals (MPa = 1 x 10^6 Pa), is more than sufficient to withstand loading of this magnitude.

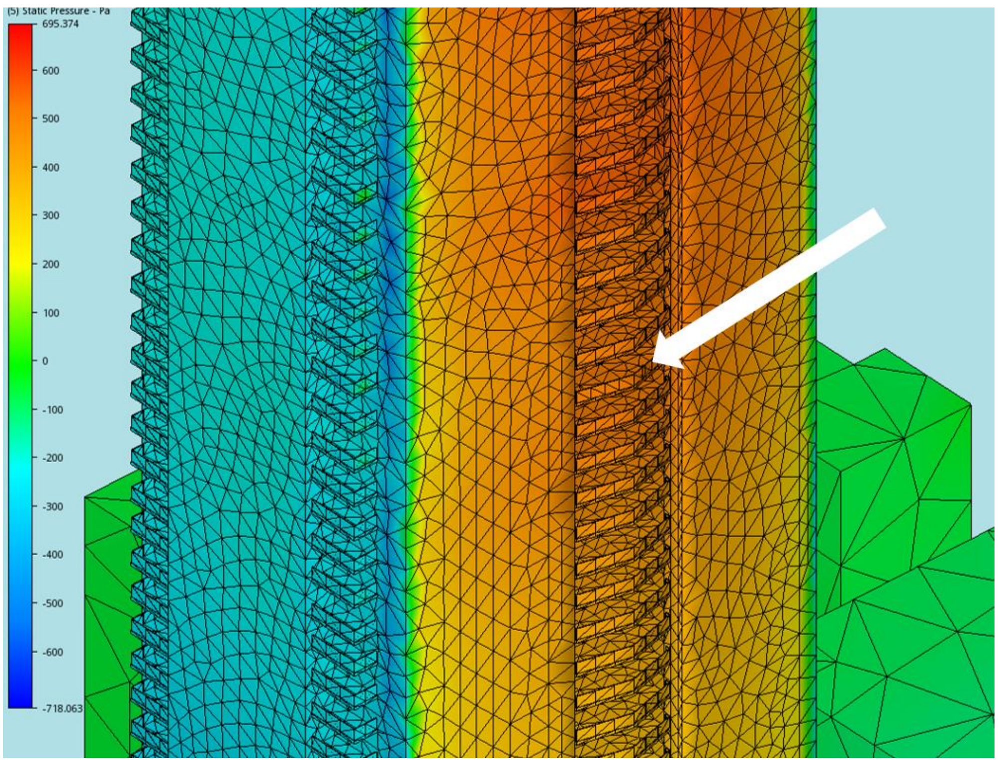

Figure 36: East facade, floor 51 failure location

It was observed that for this wind condition, failure location 2 (Floor 23/East) experiences a sheltering effect by the buildings to the East of it, and therefore does not experience any significant surface pressures.

Relatively high suction pressures are generated at the failure locations on the South façade. Failure locations 1 and 3 experience surface pressures of -247.2 Pa and -154.3 Pa, and pressure coefficients of -0.48 and -0.33 during gust conditions, respectively.

It can be seen that regions of concern identified in this simulation are the upper floors on the East façade is where surface pressures reach 500 Pa to 600 Pa under gust conditions.

Wind Direction Scenario #2: 220º

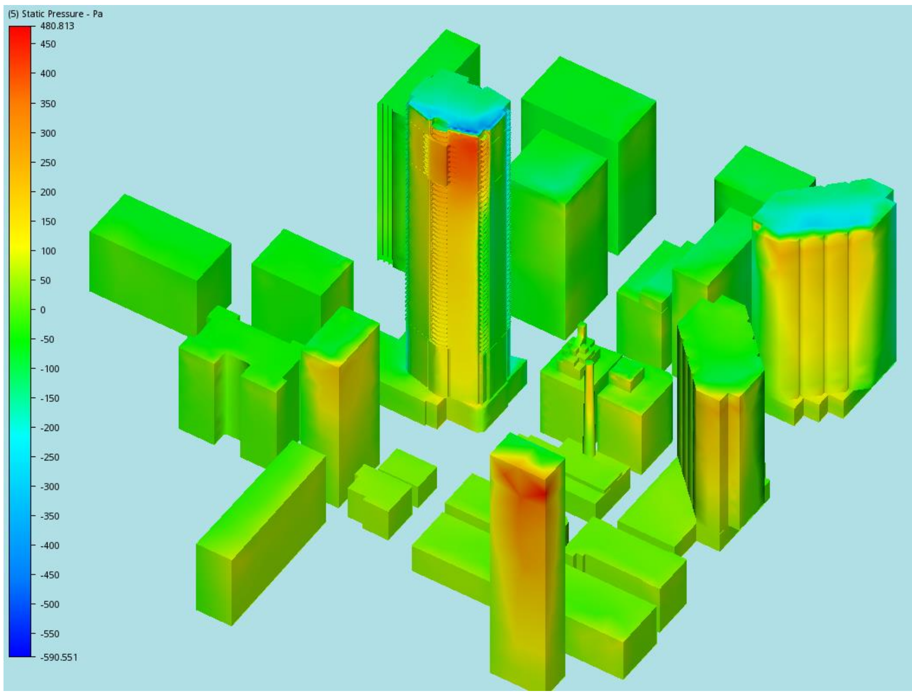

Figure 37: 220°, gust condition

Table 18: 220° CFD results

		Location 1	Location 2	Location 3	Location 4
Floor/Facade		37/South	23/East	23/South	51/East
Average Condition	Surface Pressure [Pa]	-4.4	-11.0	-1.0	-10.7
	Pressure Coefficient [-]	-0.16	-0.59	0.05	-0.31
Gust Condition (20 m/s)	Surface Pressure [Pa]	-63.8	-140.9	-7.2	-134.5
	Pressure Coefficient [-]	-0.16	-0.44	-0.02	-0.30

Number of Iterations for Solution Convergence: 756 (average), 750 (gust)

Wind from a direction of 220° resulted in suction pressures at all failure locations. The highest suction pressures were observed on the Shangri-La Hotel's East façade at failure locations 2 and 4. Locations 2 and 4 experience surface pressures of -140.9 Pa and -134.5 Pa, and pressure coefficients of -0.44 and -0.30, respectively.

It is interesting to note that the highest pressures can be observed at failure location 2 where gust conditions produce surface pressures of -140.9 Pa and a pressure coefficient of -0.44. It was predicted that higher suction pressures would be observed at failure location 4, where wind velocities are higher due to increased height. The condition produced a much higher pressure coefficient at failure location 2 than at failure location 4 (-0.44 vs. -0.30) due to this difference in freestream velocity at different heights.

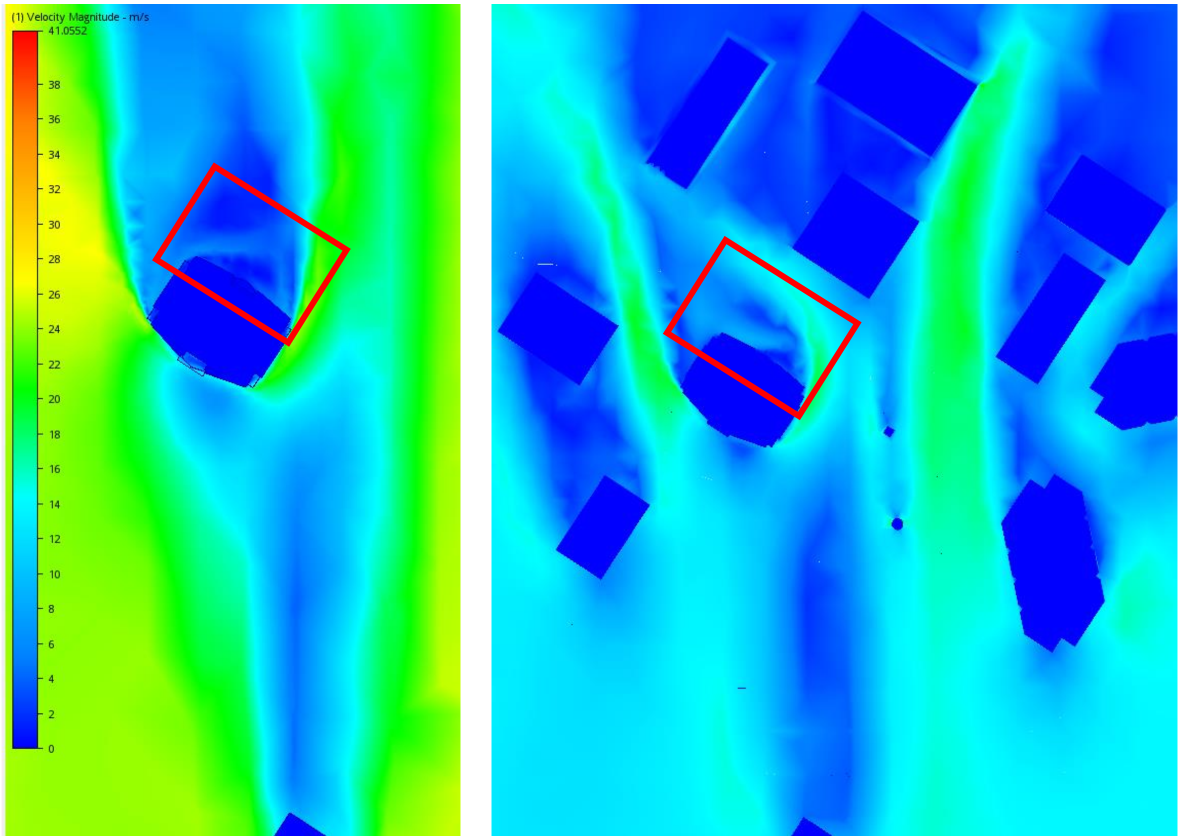

A B

Figure 38: Plan view, floor 51 (A), floor 23 (B)

It can be observed in Figure 38 that this was a result of complex flow conditions closer to street level induced by the surrounding buildings. Wind interaction between the lower buildings to the Southwest of the Shangri-La Hotel have caused an acceleration in local flow, producing higher wind speeds, on the leeward side of the Shangri-La Hotel, closer to street level. Note the higher wind speeds in the highlighted region at floor 23 level (failure location 2), compared to slower wind speeds in the highlighted region at floor 51 (failure location 4).

The results above illustrate the effect of densely packed surrounding buildings on local wind conditions close to street level. Regions of increased wind speed ("wind tunnels") between buildings can be seen developing in Figure 38 (right). Regions such as this are problematic for pedestrian comfort and must be taken into consideration in building design and urban planning.

Balconies located on the upper floors of the Southwest corner should be noted as a location of concern (Figure 39), where surface pressures are reaching 400 Pa to 450 Pa under gust condition. Also, balconies on the upper floors of the Southeast corner experience relatively high suction pressures of -200 to -250 Pa (Figure 39).

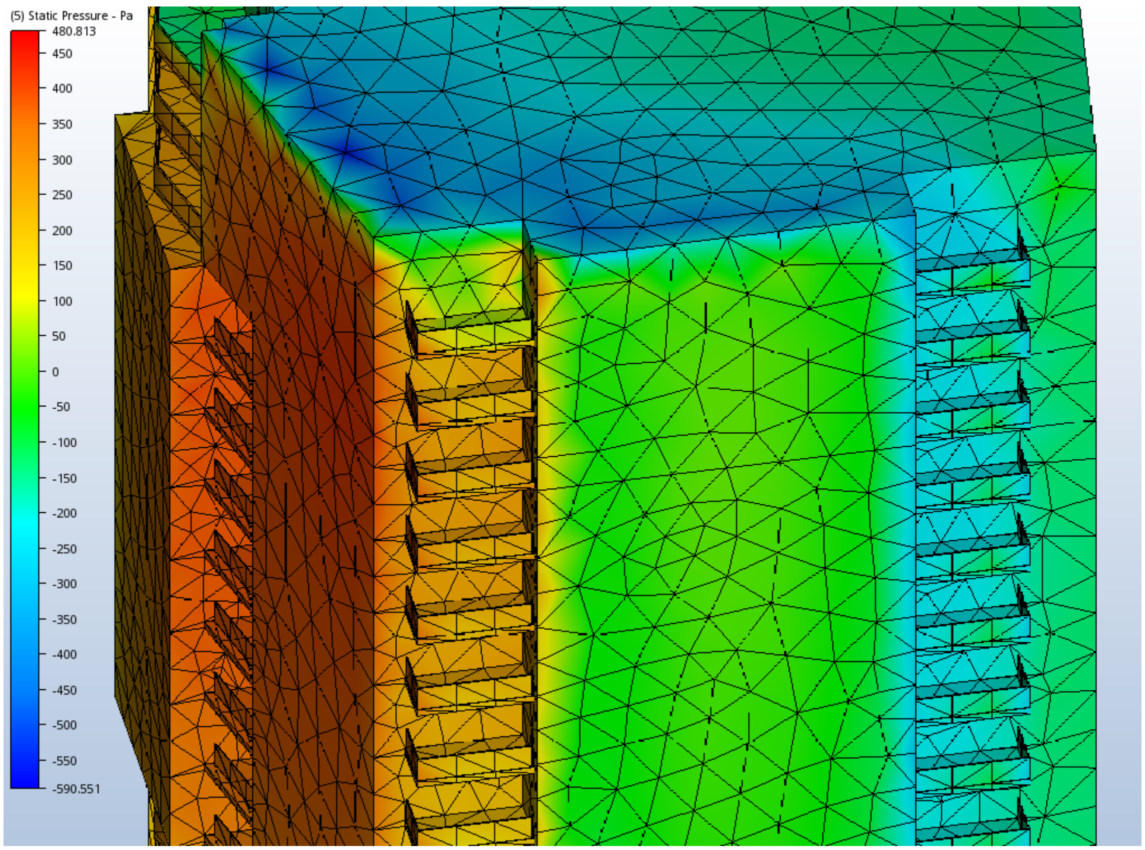

Figure 39: South facade, gust condition

Wind Direction Scenario #3: 250º

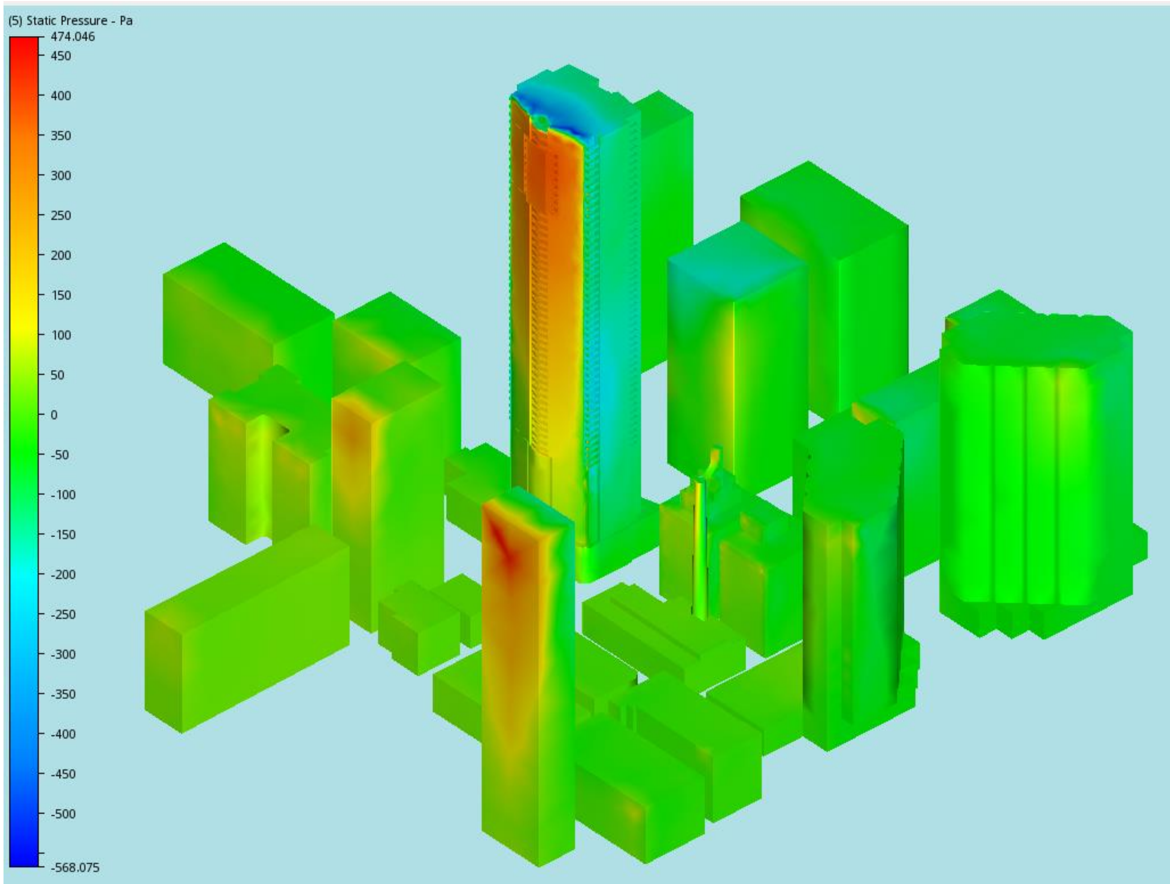

Figure 40: 250°, gust condition

Table 19: 250° CFD results

		Location 1	Location 2	Location 3	Location 4
Floor/Facade		37/South	23/East	23/South	51/East
Average Condition	Surface Pressure [Pa]	-17.2	-8.9	-12.3	-11.8
	Pressure Coefficient [-]	-0.64	-0.48	-0.66	-0.34
Gust Condition (20 m/s)	Surface Pressure [Pa]	-217.6	-136.5	-164.5	-133.8
	Pressure Coefficient [-]	-0.58	-0.44	-0.54	-0.31

Number of Iterations for Solution Convergence: 1289 (average), 856 (gust)

Wind from a direction of 250° with the same velocity conditions as scenario #2 resulted in generally higher suction pressures at all failure locations in comparison to wind direction scenario #2 (220°). Flow from this angle almost directly intersects the West façade of the Shangri-La Hotel, producing notable suction pressures on the Southwest corner. The highest suction pressure can be observed at failure location 1, where gust conditions produce an average surface pressure of -217.6 Pa and a pressure coefficient of -0.58.

Again, it is noted that on the East façade, similar pressure conditions are observed between floor 23 and floor 51, due to the acceleration of the approaching flow at near ground level as discussed in the previous section. Resulting in a higher pressure coefficient at failure location #2 (-0.44) compared to failure location #4 (-0.31). As previously mentioned, the alternating positive and negative pressures on the East façade due to the three most common wind conditions plays an important role in the fatigue loading of the balcony guards on this façade.

Balconies on the upper floors of the West façade were observed to reach surface pressures of 400 Pa to 450 Pa, and are therefore locations of concern (Figure 41).

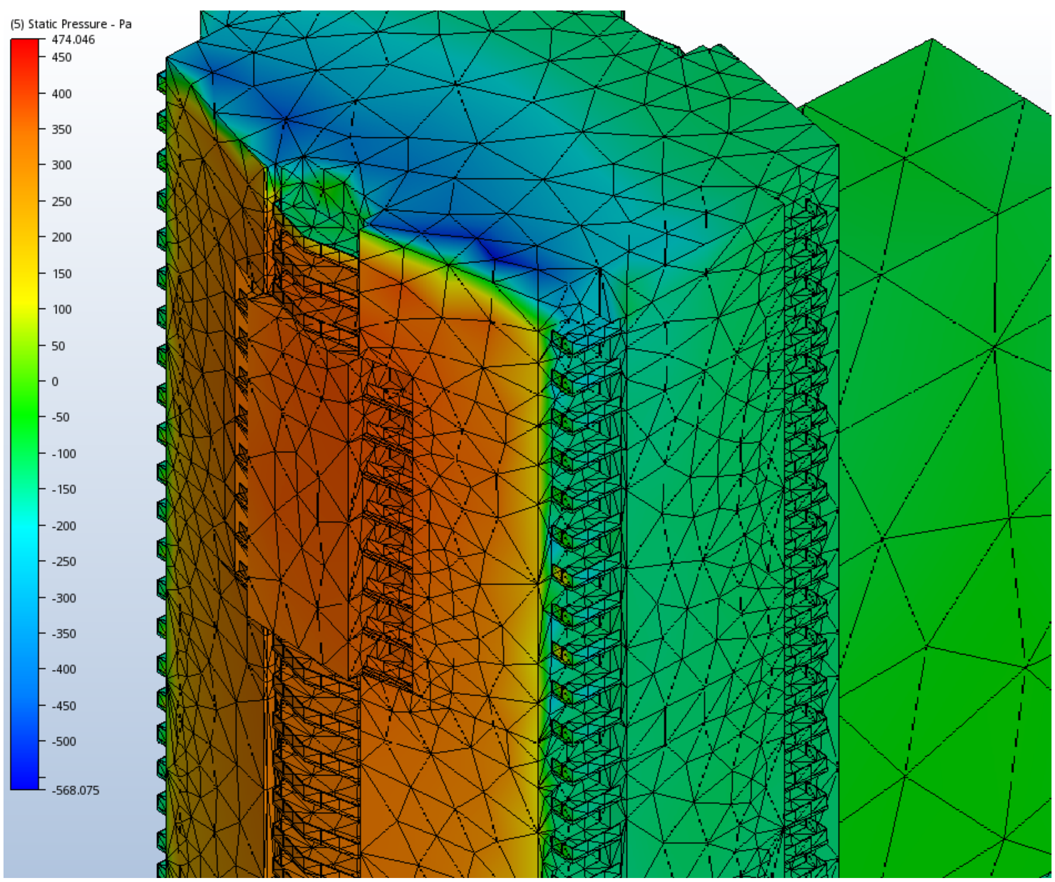

Figure 41: Southwest, gust condition

7. Conclusion

The study explored the impact of Toronto's wind conditions on glass balcony guard failures through a case study of the Shangri-La Hotel. The CFD model used to analyze the Shangri-La Hotel was successfully validated with an experimental wind tunnel study. The results of this validation study and the agreement between experimental and simulated results produced a CFD model with settings and set-up parameters that are accurate for external flow applications. The validation study demonstrated the critical need to understand the settings and set-up of simulation software in order to produce meaningful and accurate results.

It was determined that local wind conditions alone were likely not responsible for the balcony guard failures seen at the Shangri-La Hotel. From the CFD simulation results presented in Section 6.2, it can be concluded that local wind conditions produce significant positive and negative pressures on the building façade that contribute to the fatigue loading of the glass balcony guards. If any cracks or impurities, such as nickel sulphide inclusions, are embedded in the tempered glass balcony guard panels, the sustained wind conditions and gust conditions can induce failure. However, the instantaneous pressure distribution induced by local wind conditions on the building's façade does not represent a condition to which, under normal circumstances, should cause a failure of the tempered glass balcony guards. Maximum pressures simulated on the balcony surfaces were in the range of 500 Pa to 600 Pa, while tempered glass has a theoretical failure strength in the order of mega pascals (MPa = 1×10^6 Pa). A strong correlation was observed between the building's four failure locations and the most common local wind conditions determined by a historical wind data analysis. The correlation strengthens the conclusion that the local wind conditions did in fact contribute to the fatigue loading of the balcony guards and their eventual failure.

When designing tall structures, such as the Shangri-La Hotel, studies such as this must be preformed in order to understand and locate problematic areas and components of the building due to local wind conditions. In terms of existing buildings, which may be at risk of balcony guard failure, a simple study such as this can provide valuable information to building maintenance staff in regards to areas of the building that should be frequently monitored and inspected. Priority regions can be quickly identified for balcony guard replacement. For example, in the case of the Shangri-La Hotel, it would be recommended to prioritize the safeguarding and replacement of the glass balcony guards on the upper floors of the East façade.

The unfortunate reality is that impurities and defects in glass used in the construction industry are unavoidable. The impurities can produce embedded cracks that have the potential to propagate and cause failure of the glass. Propagation of the cracks becomes more likely as cyclic fatigue loading due to local wind conditions is increased and intensified. As discussed, wind conditions are intensified with height, and therefore high rise buildings are the primary building type of concern. The failure of these glass components can be mitigated by a comprehensive consideration of local wind conditions in the design process. If the wind study identifies areas of intensified wind loading, pre-emptive design choices can be made in order to prevent glass failure. For example, limited use of balconies in high wind load areas, the use of laminated glass, or the use of an alternate material such as metal in the specific regions of concern. Design features could also be incorporated which provide protection and shielding of the glass balcony guards from extreme wind conditions.

A final conclusion that can be made from this paper is that in many cases large scale wind tunnel studies are not necessary to achieve the desired results of predicting the pressure distribution along the height of the building. It was demonstrated in this paper that CFD software can be sufficient in determining and analyzing local wind patterns, and also serve as a method to visualize and approximate pressures on building facades generated by wind. This method is an inexpensive and efficient alternative to large scale wind tunnel studies.

Appendices

Appendix A

Table 20: Wind tunnel experimental data

Measurement Location	0° Orientation			10° Orientation			20° Orientation		
	Mean	Minimum	Maximum	Mean	Minimum	Maximum	Mean	Minimum	Maximum
1 (P_{C1})	229.9	221.0	238.1	224.9	217.8	231.0	225.0	217.0	232.3
2	-48.9	-135.1	75.1	22.2	-66.1	120.0	149.6	73.6	187.5
3	-29.6	-144.9	144.3	99.3	-37.1	207.3	205.4	144.0	236.1
4	45.4	-169.7	225.6	162.3	-21.1	234.0	176.1	151.1	198.9
5	-42.3	-163.6	7.6	-81.3	-265.1	24.7	-97.9	-284.8	1.6
6	-33.1	-179.0	29.5	-81.8	-325.9	55.7	-106.1	-291.6	24.2
7	-69.6	-101.4	-48.2	-81.1	-100.4	-64.8	-77.7	-92.8	-59.5
8	95.1	83.9	108.7	17.1	6.5	28.2	-48.8	-57.4	-39.9
9	-36.6	-95.9	-0.5	-37.3	-76.6	-10.4	-52.4	-109.7	-15.9
10	-34.7	-82.2	5.1	-41.2	-80.0	-11.4	-55.4	-95.9	-22.5
11	-37.3	-105.7	12.5	-41.0	-84.1	-7.0	-55.4	-107.1	-13.4
12	-41.1	-93.2	5.3	-47.6	-105.1	13.6	-63.5	-122.1	-13.9
13	147.9	129.9	162.1	211.1	203.9	217.5	206.6	201.5	211.4
14	-83.7	-219.5	44.7	-164.4	-233.0	-12.1	-101.7	-177.2	51.3
15	-31.4	-101.4	42.9	-21.1	-71.4	18.4	-31.6	-59.2	25.2
16	-57.5	-113.2	-8.7	-83.0	-136.8	-42.4	-108.3	-155.3	-64.7

*All units Pascals [Pa]

Appendix B

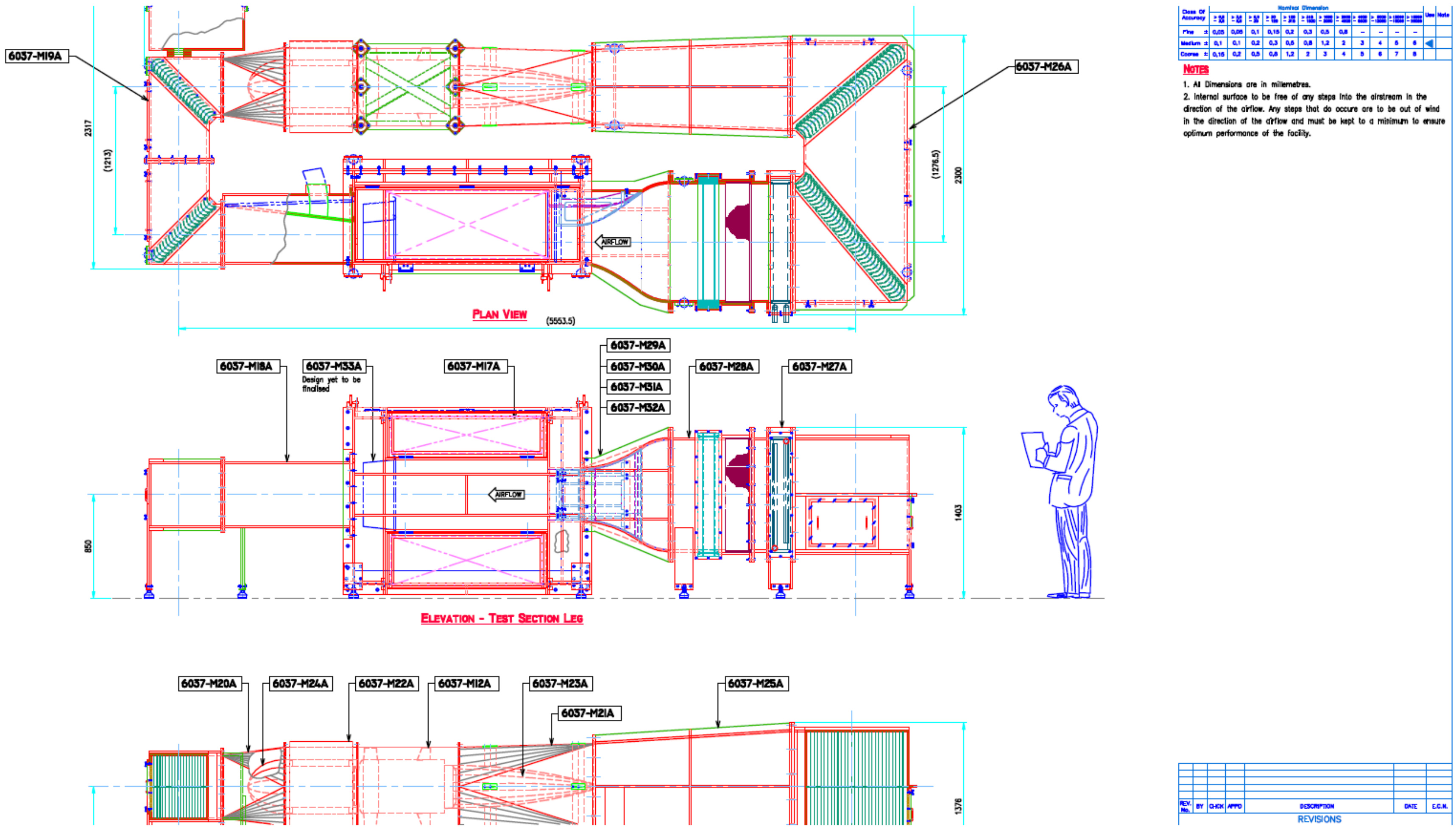

Figure 42: Wind tunnel specifications

References

[1] S. Dupont, "A simple wind-tree interaction model predicting the probability of wind damage at stand level," *Agricultural and Forest Meteorology,* pp. 49-63, 2016.

[2] T. Ihara, A. Gustavsen and B. P. Jelle, "Fatigue resistance of double sealant composed of polyisobutylene sealant adjacent to silicone sealant," *Construction and Building Materials,* vol. 66, p. 467, 2014.

[3] M. A. Mooneghi, P. Irwin and A. G. Chowdhury, "Large-scale testing on wind uplift of roof pavers," *Journal of Wind Engineering and Industrial Aerodynamics,* vol. 128, pp. 22-36, 2014.

[4] A. Kilikevičiusa, A. Čereškaa and K. Kilikevičienė, "Analysis of external dynamic loads influence to photovoltaic module structural performance," *Engineering Failure Analysis,* vol. 66, pp. 445-454, 2016.

[5] C. M. Jubayer and H. Hangan, "A numerical approach to the investigation of wind loading on an array of ground mounted solar photovoltaic (PV) panels," *Journal of Wind Engineering and Industrial Aerodynamics,* vol. 153, pp. 60-70, 2016.

[6] F. Esmaeili, T. Chakherlou and M. Zehsaz, "Prediction of fatigue life in aircraft double lap bolted joints using several multiaxial fatigue criteria," *Materials and Design,* vol. 59, pp. 430-438, 2014.

[7] J. Le, L. Song, X. Peng and X. Hu, "Fracture mechanics analysis of thermally tempered glass plate: fracture induced by an embedded crack," *International Journal of Fracture,* vol. 132(4), pp. 299-309, 2005.

[8] F. A. Veer, P. C. Louter and F. P. Bos, "The strength of annealed, heat-strengthened and fully tempered float glass," *Fatigue & Fracture of Engineering Materials & Structures,* vol. 32(1), pp. 18-25, 2008.

[9] P. R. Lehman, "The Mechanical Properties of Glass," Rutgers University, [Online]. Available: http://glassproperties.com/references/MechPropHandouts.pdf.

[10] S. Bielecki, M. Reben and J. Wasylak, "Nickel Sulphide Inclusions in Tempered Glass," *Advanced Materials Research,* Vols. 39-40, pp. 558-561, 2008.

[11] J. Chang and J. Chou, "Fracture Strength of Tempered Glass," *Journal of Non-Crystalline Solids,* vol. 52, pp. 395-404, 1982.

[12] J. Hall, "Toronto's skyline is about to join the big-leagues: What the city could look like in 2020," 2016.

[13] Glenn Research Center, "Wind Tunnel Index," [Online]. Available: https://www.grc.nasa.gov/www/k-12/airplane/shortt.html.

[14] D. Scott, R. Denoon and P. Irwin, Wind Tunnel Testing of High-Rise Buildings, Taylor and Francis, 2013.

[15] P. Irwin, R. Denoon and D. Scott, "Wind Tunnel Testing for Buildings and Other Structures," 2012.

[16] J. Hall, "The Toronto Star," 9 October 2016. [Online]. Available: https://www.thestar.com/news/insight/2016/10/09/the-art-of-taming-the-wind.html.

[17] "Wind Tunnel Testing: a General Outline," Alan G. Davenport Wind Engineering Group, London, ON, 2007.

[18] I. Chand, P. K. Bhargava and N. L. V. Krishak, "Effect of Balconies on Ventilation Inducing Aeromotive Force on Low-rise Buildings," *Building and Environment,* vol. 33, no. 6, pp. 385-396, 1998.

[19] H. Montazeri and B. Blocken, "CFD simulation of wind-induced pressure coefficients on buildings with and without balconies: Validation and sensitivity analysis," *Building and Environment,* vol. 60, pp. 137-149, 2013.

[20] D. Cabezón, E. Migoya and A. Crespo, "Comparison of turbulence models for the computational fluid dynamics simulation of wind turbine wakes in the atmospheric boundary layer," *Wind Energy,* vol. 14, no. 7, pp. 909-921, 2011.

[21] C. Teodosiu, V. Ilie and R. Teodosiu, "Appropriate CFD Turbulence Model for Improving Indoor Air Quality of Ventilated Spaces," *Mathematial Modelling in Civil Engineering,* vol. 10, no. 4, pp. 28-42, 2014.

[22] J. Zhang, S. Dembele and J. Wen, "Investigation of Turbulence Models for CFD Simulations of Gas and Liquid Pool Fires," *Journal of Fire Sciences,* vol. 27, no. 2, pp. 157-182, 2009.

[23] A. Montlaur and E. Ferrer, CFD for Wind and Tidal Offshore Turbines, Springer, 2015.

[24] B. Blocken, T. Stathopoulos and J. v. Beeck, "Pedestrian-level wind conditions around buildings: Review of wind-tunnel and CFD techniques and their accuracy for wind comfort assessment," *Building and Environment,* vol. 100, pp. 50-81, 2016.

[25] T. van Hooff, B. Blocken, L. Aanen and B. Bronsema, "A venturi-shaped roof for wind-induced natural ventilation of buildings: Wind tunnel and CFD evaluation of different design configurations," *Building and Environment,* vol. 46, no. 9, pp. 1797-1807, 2011.

[26] M. Chavez, B. Hajra, T. Stathopoulos and A. Bahloul, "Near-field pollutant dispersion in the built environment by CFD and wind tunnel simulations," *Journal of Wind Engineering and Industrial Aerodynamics,* vol. 99, no. 4, pp. 330-339, 2011.

[27] "Autodesk CFD," 2016. [Online]. Available: https://knowledge.autodesk.com/support/cfd.

[28] T. Perkins, "Toronto leads North American high-rise construction," 2012.

[29] "Report of the Expert Panel on Glass Panels in Balcony Guards," Ontario Ministry of Health and Long-Term Care, 2012.

[30] "Supplementary Standard SB-13 Glass in Guards," 2012.

[31] G. Hildebrand and P. Vegh, "Guards in Buildings - The Canadian Challenge," in *14th Canadian Conference on Building Science and Technology*, 2014.

[32] Wind Tunnel Testing Standards Committee, Wind Tunnel Testing for Buildings and Other Structures, ASCE, 2012.

[33] N. B. Hutcheon and G. O. Handegord, Building Science for a Cold Climate, Construction Technology Centre Atlantic Inc., 1995.